

Testing cosmic acceleration for $w(z)$ parameterizations using f_{gas} measurements in galaxy clusters

Juan Magaña^{1*}, V. Motta^{1†}, Víctor H. Cárdenas^{1‡}, and G. Foëx^{1,2§}

¹*Instituto de Física y Astronomía, Facultad de Ciencias, Universidad de Valparaíso, Avda. Gran Bretaña 1111, Valparaíso, Chile.*

²*Max Planck Institute for Extraterrestrial Physics, Giessenbachstrasse, 85748 Garching, Germany*

2 March 2022

ABSTRACT

In this paper we study the cosmic acceleration for five dynamical dark energy models whose equation of state varies with redshift. The cosmological parameters of these models are constrained by performing a MCMC analysis using mainly gas mass fraction, f_{gas} , measurements in two samples of galaxy clusters: one reported by Allen et al. (2004), which consists of 42 points spanning the redshift range $0.05 < z < 1.1$, and the other by Hasselfield et al. (2013) from the Atacama Cosmology Telescope survey, which consists of 91 data points in the redshift range $0.118 < z < 1.36$. In addition, we perform a joint analysis with the measurements of the Hubble parameter $H(z)$, baryon acoustic oscillations and the cosmic microwave background radiation from WMAP and Planck measurements to estimate the equation of state parameters. We obtained that both f_{gas} samples provide consistent constraints on the cosmological parameters. We found that the f_{gas} data is consistent at the 2σ confidence level with a cosmic slowing down of the acceleration at late times for most of the parameterizations. The constraints of the joint analysis using WMAP and Planck measurements show that this trend disappears. We have confirmed that the f_{gas} probe provides competitive constraints on the dark energy parameters when a $w(z)$ is assumed.

Key words: dark energy, cosmological parameters, galaxy clusters

1 INTRODUCTION

The standard cosmological paradigm states that the Universe evolves from a decelerated to an accelerated phase at late times. The evidence of this cosmic acceleration (CA) comes not only from type Ia supernova (SNIa) (Perlmutter et al. 1999; Riess et al. 1998), but also from several other cosmological observations (Mortonson et al. 2014; Davis 2014; Li et al. 2013; Albrecht et al. 2006).

There are two approaches to explain this feature of the Universe: one is to modify the right hand side of Einstein’s equation by assuming the existence of an energy source, dubbed dark energy (DE), that produces these effects, and the other is to modify the left hand side by modifying the gravity theory (Joyce et al. 2016). The main property of the DE source that generates the CA is an equation of state (EoS) parameter w , which is the ratio between its pressure and energy density. When $w = -1$ we obtain the well-known cosmological constant, Λ .

The Λ cold dark matter (Λ CDM) model satisfactorily explains the CA. However it presents several unsolved problems, i.e., the 120 orders of magnitude between the quantum field theory prediction and the cosmological measurements and why the DE density is similar to that of dark matter (DM) today (Weinberg 1989; Copeland, Sami & Tsujikawa 2006). Additionally, the increase in number and precision of cosmological observations has allowed confronting and explore beyond the standard Λ CDM (Di Valentino et al. 2015; Gong, Gao & Zhu 2013; Magaña et al. 2015; Marra et al. 2013; Planck collaboration 2013).

One of the methods used to explore departures from the Λ CDM model is to assume a redshift dependent EoS parameter $w(z)$, given by a suitable parameterization. The most used parameterization for $w(z)$ is the Chevallier-Polarski-Linder (CPL) ansatz (Chevallier & Polarski 2001; Linder 2003) that expands $w(z) = w_0 + w_1 z / (1 + z)$, where w_0 is the present value of the EoS and w_1 is its derivative with respect to redshift.

An intriguing feature emerges once the CPL function for $w(z)$ is used with SNIa. Shafieloo, Sahni & Starobinsky (2009) found evidence of a low redshift transition of the reconstructed deceleration parameter $q(z)$, the so called slowing down of the CA, that shows a turn around at $z \sim 0.3$

* juan.magana@uv.cl

† veronica.motta@uv.cl

‡ victor.cardenas@uv.cl

§ gfoex@mpe.mpg.de

(see also Guimarães & Lima 2011). We have found that such a feature does not only appear with SNIa but also with gas mass fraction (f_{gas}) data in clusters (Cárdenas, Bernal & Bonilla 2013).

Furthermore, another curious behavior emerges when the high redshift data sets are taken into account (as cosmic microwave background radiation, CMB, or baryon acoustic oscillations, BAO): the transition feature at low redshift disappears, making it consistent with the Λ CDM model (Shafieloo, Sahni & Starobinsky 2009; Li, Wu & Yu 2011; Cárdenas & Rivera 2012; Cárdenas, Bernal & Bonilla 2013). Then, the key point is to separate the low redshift and high redshift data to study this effect.

Magaña, Cárdenas & Motta (2014) investigated this trend in $q(z)$ for five different EoS parameterizations using also four SNIa data sets; the Constitution (Hicken et al. 2009), Union 2 (Amanullah et al. 2010), Union 2.1 (Susuki et al. 2012) and Lick Observatory Supernova Search (LOSS) (Ganeshalingam, Li & Filippenko 2013) SNIa samples. They found that, using only SNIa data, the acceleration of the Universe seems to have already peaked and it is evolving towards lower rates of acceleration. This result is independent of the EoS parameterization used and it is observed in the Constitution, Union 2 and LOSS data sets. However, this behavior disappears when the Union 2.1 sample is used. As in previous studies, if the cosmological observations at high redshift are included in the analysis, the results change $q(z)$ from a decelerated to an accelerated phase, very similar to the case of the cosmological constant.

Recently, Wang et al. (2015) performed a similar analysis for several $w(z)$ functions using the latest cosmological data from SNIa, CMB and BAO. As in Magaña, Cárdenas & Motta (2014), the authors confirm that the evolution of CA is independent of the EoS parameterization. In addition, they found that the Legacy Survey (SNLS3, Conley et al. 2011) SNIa data favors the slowing down of the CA while the Joint Light-Curve Analysis (JLA, Betoule et al. 2014) sample prefers an eternal CA. They also shown that the effects of different BAO data on CA are negligible. By revisiting the role of the spatial curvature, Wang et al. (2015) found that a non-flat Universe prefers a slowing down of the CA. This result is consistent with those obtained by Cárdenas & Rivera (2012). An interesting result is that the Planck 2015 data (Planck collaboration 2015,b) favored the slowing down of the CA, while in previous works, this trend disappears when the CMB data is taken into account in the analysis.

Here we are interested in testing the transition in the cosmic acceleration as well as the possibility of the slowing down in the acceleration for dynamical DE with a $w(z)$ parameterization using galaxy clusters observations. Several authors have addressed that the gas mass fraction measurements in galaxy clusters can be used to put constraints on cosmological models (Sasaki 1996; Allen et al. 2004; Bonamente et al. 2006; Allen et al. 2008; LaRoque et al. 2006; Ettori et al. 2009; Mantz et al. 2014). Therefore, f_{gas} data constitute a complementary geometric method to constrain the parameter space of the same EoS parameterizations studied in Magaña, Cárdenas & Motta (2014).

The paper is organized as follows: in the next section we introduce the cosmological framework for a flat Universe case. In section §3 we present the $w(z)$ parameterizations. In section §4 we describe the methodology and data used

to constrain the parameters of the models. In section §5 we present and discuss the results. Finally, we present our conclusions in section §6.

2 COSMOLOGICAL FRAMEWORK

We consider a flat Friedmann-Lemaître-Robertson-Walker (FLRW) Universe with scale factor a and whose DE component has a dynamical EoS $w(z)$. The dimensionless Hubble parameter $E(z)$ for this Universe is given by

$$E^2(z) \equiv H^2(z)/H_0^2 = \Omega_m(1+z)^3 + \Omega_r(1+z)^4 + \Omega_{de}X(z), \quad (1)$$

where $H_0 = H(0) = h \times 100 \text{ km s}^{-1} \text{ Mpc}^{-1}$, Ω_m and Ω_r are the density parameter at present day for matter and radiation respectively. We compute $\Omega_r = 2.469 \times 10^{-5} h^{-2} (1 + 0.2271 N_{eff})$, where $N_{eff} = 3.04$ is the standard number of relativistic species (Komatsu et al. 2011). The density parameter for DE is written as $\Omega_{de} = 1 - \Omega_m - \Omega_r$, and the function $X(z)$ reads as

$$X(z) \equiv \frac{\rho_{de}(z)}{\rho_{de}(0)} = \exp\left(3 \int_0^z \frac{1+w(z)}{1+z} dz\right), \quad (2)$$

where $\rho_{de}(z)$ is the energy density of DE at redshift z , and $\rho_{de}(0)$ its present value. The comoving distance from the observer to redshift z is given by

$$r(z) = \frac{c}{H_0} \int_0^z \frac{dz'}{E(z')}, \quad (3)$$

and it is related to the angular diameter distance as

$$D_A(z) = \frac{r(z)}{(1+z)}. \quad (4)$$

Since we are interested in testing the CA for dynamical DE models, we study the deceleration parameter $q(z)$ defined as

$$q(z) = -\frac{\ddot{a}(z)a(z)}{\dot{a}^2(z)}, \quad (5)$$

where the dot stands for the derivative with respect to the cosmic time. Using eq. (1), this expression can be rewritten as

$$q(z) = \frac{(1+z)}{E(z)} \frac{dE(z)}{dz} - 1. \quad (6)$$

3 $w(z)$ PARAMETERIZATIONS

One natural extension to the cosmological constant is to explore dynamical DE where the EoS parameter $w(z)$ varies with redshift through an explicit parameterization. Here we consider the following five parameterizations: Jassal-Bagla-Padmanabhan (JBP, Jassal, Bagla & Padmanabhan 2005a,b), Barbosa-Alcaniz (BA, Barboza & Alcaniz 2008), Feng-Shen-Li-Li (FSLL, Feng, Shen, Li & Li 2012), and Sendra-Lazkoz (SL, Sendra & Lazkoz 2012)

Parameterization	$w(\infty)$	$X(z)$
JBP	w_0	$(1+z)^{3(1+w_0)} \exp\left[\frac{3}{2} \frac{w_1 z^2}{(1+z)^2}\right]$
BA	$w_0 + w_1$	$(1+z)^{3(1+w_0)} (1+z^2)^{\frac{3}{2} w_1}$
FSLL I	w_0	$(1+z)^{3(1+w_0)} \exp\left[\frac{3w_1}{2} \arctan(z)\right] (1+z^2)^{\frac{3}{4} w_1} (1+z)^{-\frac{3}{2} w_1}$
FSLL II	$w_0 + w_1$	$(1+z)^{3(1+w_0)} \exp\left[-\frac{3w_1}{2} \arctan(z)\right] (1+z^2)^{\frac{3}{4} w_1} (1+z)^{\frac{3}{2} w_1}$
SL	$\frac{1}{2}(-1 - 8w_0 + 9w_{0.5})$	$(1+z)^{\frac{3}{2}(1-8w_0+9w_{0.5})} \exp\left[\frac{3z\{w_0(52z+40)-9w_{0.5}(5z+4)+7z+4\}}{8(1+z)^2}\right]$

Table 1. Properties for each $w(z)$ parameterization. The second column shows the amplitude of $w(z)$ when $z \rightarrow \infty$. The third column shows the function $X(z)$ given by the Eq. (2)

$$w(z) = w_0 + w_1 \frac{z}{(1+z)^2} \quad \text{JBP}, \quad (7)$$

$$w(z) = w_0 + w_1 \frac{z(1+z)}{1+z^2} \quad \text{BA}, \quad (8)$$

$$w(z) = w_0 + w_1 \frac{z}{1+z^2} \quad \text{FSLL I}, \quad (9)$$

$$w(z) = w_0 + w_1 \frac{z^2}{1+z^2} \quad \text{FSLL II}, \quad (10)$$

$$w(z) = -1 + c_1 \left(\frac{1+2z}{1+z}\right) + c_2 \left(\frac{1+2z}{1+z}\right)^2 \quad \text{SL}, \quad (11)$$

where $w_0 = w(0)$ for all parameterizations, $w_1 = w'(0)$ (' denotes derivative with respect to redshift), the constant $c_1 = (16w_0 - 9w_{0.5} + 7)/4$, and $c_2 = -3w_0 + (9w_{0.5} - 3)/4$, being $w_{0.5}$ the value of the EoS when $z = 0.5$. Table 1 shows the amplitude of the EoS when $z \rightarrow \infty$ and the function $X(z)$ given by Eq. (2) for each parameterization.

4 METHODOLOGY AND DATA

The EoS parameters for each $w(z)$ function are constrained by performing a Markov Chain Monte Carlo (MCMC) analysis using the following cosmological observations: the f_{gas} measurements in galaxy clusters, $H(z)$ estimations, BAO data, and the CMB information.

4.1 The gas mass fraction in galaxy clusters

4.1.1 f_{gas} modeling data

The gas mass fraction is defined as $f_{\text{gas}} \equiv M_{\text{gas}}/M_{\text{tot}}$, where M_{gas} is the X-ray gas mass and M_{tot} is the dynamical total mass of the galaxy cluster. The f_{gas} is useful as a cosmological probe when a scaling relation between the baryonic gas mass fraction in galaxy clusters and the global fraction of baryonic matter and dark matter of the Universe Ω_b/Ω_{0m} is assumed. The f_{gas} estimations for any cosmological model fitted to the reference Λ CDM data can be obtained by writing M_{gas} and M_{tot} in terms of $D_A(z)$ (Sasaki 1996; Nesseris & Perivolaropoulos 2007):

$$f_{\text{gas}}(z) \equiv \frac{b}{1+\alpha} \frac{\Omega_b}{\Omega_m} \left(\frac{D_A^{\Lambda\text{CDM}}(z)}{D_A(z)}\right)^{3/2}, \quad (12)$$

where $D_A(z)$ is the angular diameter distance for any cosmological model, $D_A^{\Lambda\text{CDM}}(z)$ is the angular diameter distance for the Λ CDM reference model, Ω_b is the baryonic density parameter, and Ω_m is the current DM density parameter. Here b is a bias factor which relates the baryonic fraction in clusters with the one in the Universe. The constant α relates the baryonic luminous mass and the baryonic gas mass. This constant is $\alpha \approx 0.19\sqrt{h}$ (Allen et al. 2004). Hereafter, we refer to the fitting function given by the Eq. (12) as A04. From here on, we assume that the gas mass fraction measurements are uncorrelated. To constrain the parameters of the $w(z)$ functions introduced in §3, we use the following chi-square in the MCMC analysis

$$\chi_{f_{\text{gas}}}^2 = \left(\sum_{i=1}^N \frac{[f_{\text{gas}}(z_i) - f_{\text{gas}}^{\text{obs}}(z_i)]^2}{\sigma_{f_{\text{gas},i}}^2}\right) + \left(\frac{h - h_{\text{prior}}}{\sigma_{h,\text{prior}}}\right)^2 + \left(\frac{\Omega_b h^2 - \Omega_b h_{\text{prior}}^2}{\sigma_{\Omega_b h^2, \text{prior}}}\right)^2 + \left(\frac{b - 0.824}{0.089}\right)^2, \quad (13)$$

where $f_{\text{gas}}(z)$ is calculated using A04, $f_{\text{gas}}^{\text{obs}}$ is the observed gas mass fraction, and $\sigma_{f_{\text{gas}}}$ is the error in the measurements. $N = 42$ (91) for the Allen (ACT) data set. Table 2 gives the adopted priors for h and $\Omega_b h^2$ from WMAP (Hinshaw et al. 2013) and Planck measurements (Planck collaboration 2013).

Allen et al. (2008) modified the Eq. (12) to include more corrections related to the cluster physics and the cosmological model as:

$$f_{\text{gas}}(z) = \frac{KA\gamma b(z)}{1+s(z)} \left(\frac{\Omega_b}{\Omega_m}\right) \left[\frac{D_A^{\Lambda\text{CDM}}(z)}{D_A(z)}\right]^{1.5}. \quad (14)$$

The factor A in Eq. (14) is given by

$$A = \left(\frac{\theta_{2500}^{\Lambda\text{CDM}}}{\theta_{2500}}\right)^\eta \approx \left(\frac{H(z)D_A(z)}{[H(z)D_A(z)]^{\Lambda\text{CDM}}}\right)^\eta, \quad (15)$$

which accounts for the change in the angle subtended by r_{2500} ¹ as the underlying cosmology is varied. Here, η is the slope of the f_{gas} data in the region of r_{2500} as measured for the reference Λ CDM cosmology. The parameter γ takes into account the non-thermal pressure support in the clusters. The parameter $s(z) = s_0(1+s_1z)$ models the baryonic mass fraction in stars as function of redshift. The bias factor

¹ the radius within which the cluster average density is 2500 times the critical density.

Parameter	Allowance
h	0.73 ± 0.0175 (Gaussian)
$\Omega_b h^2$	0.02202 ± 0.00046 (Gaussian)
Ω_m	$[0.2, 0.4]$ (Uniform)
w_0	$[-2, 0]$ (Uniform)
$w_1(w_{0.5})$	$[-10, 2]$ (Uniform)
A04	
b	0.824 ± 0.089 (Gaussian)
A08	
η	0.214 ± 0.022 (Gaussian)
γ	$1.0 < \gamma < 1.1$ (Uniform)
$s_0/h_{70}^{0.5}$	0.16 ± 0.048 (Gaussian)
s_1	$-0.2 < s_1 < 0.2$ (Uniform)
b_0	$0.65 < b_0 < 1.0$ (Uniform)
b_1	$-0.1 < b_1 < 0.1$ (Uniform)
K	1.0 ± 0.1 (Gaussian)

Table 2. Priors on h (Riess et al. 2016), $\Omega_b h^2$ (Cooke et al. 2014), and the different parameters of the fitting functions A04 (Eq. 12, Allen et al. 2004) and A08 (Eq. 14, Allen et al. 2008)

also depends on the redshift as $b(z) = b_0(1 + b_1 z)$. K parameterizes the residual uncertainty in the accuracy of the instrument calibration and X-ray modelling. Hereafter, we refer to f_{gas} function given by the Eq. (14) as A08. We also consider the fitting function A08 to estimate (Table 2 lists the adopted priors for A08) the EoS parameters using

$$\begin{aligned} \chi_{f_{\text{gas}}}^2 &= \left(\sum_{i=1}^N \frac{[f_{\text{gas}}(z_i) - f_{\text{gas}}^{\text{obs}}(z_i)]^2}{\sigma_{f_{\text{gas},i}}^2} \right) + \left(\frac{h - h_{\text{prior}}}{\sigma_{h,\text{prior}}} \right)^2 \\ &+ \left(\frac{\Omega_b h^2 - \Omega_b h_{\text{prior}}^2}{\sigma_{\Omega_b h^2, \text{prior}}} \right)^2 + \left(\frac{\eta - 0.214}{0.022} \right)^2 \\ &+ \left(\frac{s_0 / \sqrt{(100/70)h} - 0.16}{0.048} \right)^2 + \left(\frac{K - 1.0}{0.1} \right)^2. \end{aligned} \quad (16)$$

4.1.2 f_{gas} samples

We use two galaxy cluster gas mass fraction samples: the sample by Allen et al. (2004), $f_{\text{gas}}^{\text{Allen}}$, which consists of 42 points spanning the redshift range $0.05 < z < 1.1$ and the ACT sample, $f_{\text{gas}}^{\text{ACT}}$, which consists of 91 data points in the redshift range $0.118 < z < 1.36$. While Allen et al. (2004) provide the f_{gas} measurements, the ACT sample gives the mass² M_{500} calculated using the one-parameter family of universal pressure profiles for the cluster gas (Hasselfield et al. 2013). The relation between M_{500} and f_{gas} is (see Gonçalves et al. 2015; Vikhlinin et al. 2009, for more details).

$$f_{\text{gas}} = (0.0764 \pm 0.004) h^{-1.5} + (0.037 \pm 0.006) \log M_{15}, \quad (17)$$

where M_{15} is the cluster total mass, M_{500} , in units of $10^{15} h^{-1} M_{\odot}$. Notice the computed f_{gas} data points could be biased due to the Eq. (17), since it depends on a fiducial cosmology. In addition, the constraints also could be deteriorated due to the intrinsic scatter in the scaling relation. In Appendix A we study the impact of considering 15% error

² The mass M_{500} is defined as the one measured within the radius R_{500} at which the enclosed mean density is 500 times the critical density at the cluster redshift.

(3σ) in each parameter of the Eq. 17 for the JBP model. We show that the best fits obtained are within the 1σ confidence level.

4.2 $H(z)$ measurements

Our Bayesian analysis also considers the measurements of the Hubble parameter which is directly related to the expansion history of the Universe. We used 34 points in the redshift range $0.07 \leq z \leq 2.3$ compiled by Sharov & Vorontsova (2014) (see also Farooq & Ratra 2013 and Chen et al. 2013). The data set is shown in Table D1 of the Appendix D. It is worth to notice that some $H(z)$ points might be correlated to BAO measurements, i.e. BAO points together with the best fit value of the sound horizon from CMB data could be used to estimate the $H(z)$ value. Although some of the $H(z)$ points in the Table 3 were obtained in this manner, through this work we assume there is no correlation between $H(z)$ and BAO. Then, the χ_H^2 can be written as

$$\chi_H^2 = \sum_{i=1}^{34} \frac{[H(z_i) - H_{\text{obs}}(z_i)]^2}{\sigma_{H_i}^2}, \quad (18)$$

where $H_{\text{obs}}(z_i)$ is the observational Hubble parameter at z_i , σ_{H_i} its error, and $H(z_i)$ is the theoretical value for a model.

4.3 BAOs measurements

Another independent test to put constraints on cosmological parameters is to use the BAO signature. The BAO measurements considered in our analysis are obtained from the Six-degree-Field Galaxy Survey (6dFGS) BAO data (Beutler et al. 2011), the WiggleZ experiment (Blake et al. 2011), the Sloan Digital Sky Survey (SDSS) Data Release 7 (DR7) BAO distance measurements (Percival et al. 2010), the Baryon Oscillation Spectroscopic Survey (BOSS) SDSS Data Release 9 BAO distance measurements (SDSS DR9) (Anderson et al. 2012) and the most recent BAO distance estimations from Data release 11 (DR11) of the BOSS (quasars) of SDSS. WiggleZ points are obtained using the low redshift data from SDSS and 6dFGS, thus they might be correlated. Nevertheless, in this work we assume that they are not correlated.

The 6dFGS BAO estimated the distance ratio $d_z = 0.336 \pm 0.015$ at $z = 0.106$ (Beutler et al. 2011), where

$$d_z = \frac{r_d}{D_V(z)}, \quad (19)$$

where $r_d = r_s(z_d)$ and the distance scale D_V is defined as

$$D_V(z) = \frac{1}{H_0} \left[(1+z)^2 D_A(z)^2 \frac{cz}{E(z)} \right]^{1/3}. \quad (20)$$

In the standard scenario $D_A(z)$ relates to the luminosity distance through $D_A(z) = D_L(z)/(1+z)^2$. The comoving sound horizon, $r_s(z)$, is defined as

$$r_s(z) = c \int_z^{\infty} \frac{c_s(z')}{H(z')} dz', \quad (21)$$

where the sound speed $c_s(z) = 1/\sqrt{3(1 + \bar{R}_b/(1+z))}$, with $\bar{R}_b = 31500 \Omega_b h^2 (T_{\text{CMB}}/2.7\text{K})^{-4}$, and T_{CMB} is the CMB temperature.

The redshift z_d at the baryon drag epoch is well fitted with the formula proposed by Eisenstein & Hu (1998),

$$z_d = \frac{1291(\Omega_m h^2)^{0.251}}{1 + 0.659(\Omega_m h^2)^{0.828}} [1 + b_1(\Omega_b h^2)^{b_2}], \quad (22)$$

where

$$b_1 = 0.313 (\Omega_m h^2)^{-0.419} [1 + 0.607 (\Omega_m h^2)^{0.674}], \quad (23)$$

$$b_2 = 0.238 (\Omega_m h^2)^{0.223}. \quad (24)$$

It is worth to note that these equations were calculated for the standard cosmology, here we assume that they are valid for dynamical DE models. Therefore, the chi-square for the 6dFGS BAO measurement is given by

$$\chi_{6dFGS}^2 = \left(\frac{d_z - 0.336}{0.015} \right)^2. \quad (25)$$

From WiggleZ, Kazin et al. (2014, see also Gong et al. 2015) estimated the following three points for $d_z = 0.0870 \pm 0.0042$, 0.0672 ± 0.0031 , and 0.0593 ± 0.0020 at redshifts $z = 0.44, 0.6$ and 0.73 respectively.

Thus, the χ^2 for the WiggleZ BAO data is given by

$$\begin{aligned} \chi_{\text{WiggleZ}}^2 &= \left(\frac{d_z(0.44) - 0.0870}{0.0042} \right)^2 \\ &+ \left(\frac{d_z(0.6) - 0.0672}{0.0031} \right)^2 \\ &+ \left(\frac{d_z(0.73) - 0.0593}{0.0020} \right)^2. \end{aligned} \quad (26)$$

Similarly, using the clustering of galaxies from SDSS DR7, Ross et al. (2015, see also Percival et al. 2010) obtained a consensus measurement $D_V = (664 \pm 25)(r_d/r_{d, fid})$ Mpc of the BAO scale at $z = 0.15$. By adopting the value of the fiducial cosmology $r_{d, fid}$ and inverting, Gong et al. (2015) estimate d_z and the χ^2 can be expressed as

$$\chi_{\text{DR7}}^2 = \left(\frac{d_z(0.15) - 0.2239}{0.0084} \right)^2, \quad (27)$$

Anderson et al. (2014, see also Anderson et al. 2012) measure the BAO signature from the SDSS-III BOSS DR11 and give the consensus estimations for the distance $D_v = (1264 \pm 25 \text{Mpc})(r_d/r_{d, fid})$ at redshift $z = 0.32$ and $D_v = (2056 \pm 20 \text{Mpc})(r_d/r_{d, fid})$ at redshift $z = 0.57$. Using the $r_{d, fid}$ value given by the authors and inverting to obtain d_z , the χ^2 is written as

$$\chi_{\text{DR11a}}^2 = \left(\frac{d_z(0.32) - 0.1181}{0.0023} \right)^2 + \left(\frac{d_z(0.57) - 0.0726}{0.0007} \right)^2, \quad (28)$$

The most recent measured position of the BAO peak from SDSS DR11 determines $D_H/r_d = 9.18 \pm 0.28$ at $z = 2.34$ (Delubac et al. 2014), and $D_H/r_d = 9.0 \pm 0.3$ at $z = 2.36$ (Font-Ribera et al. 2014) where $D_H(z) = c/H(z)$. Thus, we compute the χ^2 for these points as

$$\chi_{\text{DR11b}}^2 = \left(\frac{\frac{D_H(2.34)}{r_d} - 9.18}{0.28} \right)^2 + \left(\frac{\frac{D_H(2.36)}{r_d} - 9.00}{0.3} \right)^2. \quad (29)$$

The total χ^2 for all the BAO data points can be written as

$$\chi_{\text{BAO}}^2 = \chi_{6dFGS}^2 + \chi_{\text{WiggleZ}}^2 + \chi_{\text{DR7}}^2 + \chi_{\text{DR11a}}^2 + \chi_{\text{DR11b}}^2. \quad (30)$$

4.4 CMB

We also include CMB information by using the following distance posteriors: the acoustic scale, l_A , the shift parameter, R , and the decoupling redshift, z_* . These quantities can be used to constrain cosmological parameters without considering the full CMB measurements (Komatsu et al. 2009, 2011; Wang & Mukherjee 2006; Wright 2007). Although these distance posterior are computed assuming an underlying cosmology, several authors have proved that these quantities are almost independent on the input DE models (Li et al. 2008; Mukherjee et al. 2008; Wang et al. 2012; Planck collaboration 2015b).

The acoustic scale is defined as

$$l_A = \frac{\pi r(z_*)}{r_s(z_*)}, \quad (31)$$

where the redshift of decoupling z_* is given by (Hu & Sugiyama 1996),

$$z_* = 1048 [1 + 0.00124(\Omega_b h^2)^{-0.738}] [1 + g_1(\Omega_m h^2)^{g_2}], \quad (32)$$

and

$$\begin{aligned} g_1 &= \frac{0.0783(\Omega_b h^2)^{-0.238}}{1 + 39.5(\Omega_b h^2)^{0.763}}, \\ g_2 &= \frac{0.560}{1 + 21.1(\Omega_b h^2)^{1.81}}. \end{aligned} \quad (33)$$

It is worth to note that we assume that these fitting formulae are valid in dynamical DE models. The shift parameter is defined as (Bond, Efstathiou & Tegmark 1997)

$$R = \frac{\sqrt{\Omega_m H_0^2}}{c} r(z_*). \quad (34)$$

Thus, the χ^2 for the CMB data is constructed as

$$\chi_{\text{CMB}}^2 = X^T \text{Cov}_{\text{CMB}}^{-1} X, \quad (35)$$

where $\text{Cov}_{\text{CMB}}^{-1}$ is the inverse covariance matrix and

$$X = \begin{pmatrix} l_A^{th} - l_A^{obs} \\ R^{th} - R^{obs} \\ z_*^{th} - z_*^{obs} \end{pmatrix}, \quad (36)$$

the superscripts *th* and *obs* refer to the theoretical and observational estimations respectively.

Hinshaw et al. (2013) obtained for a flat Λ CDM Universe, using the WMAP 9-yr temperature power spectrum, the following distance posteriors $l_A^{obs} = 302.40$, $R^{obs} = 1.7246$, $z_*^{obs} = 1090.88$, and the inverse covariance matrix

$$\text{Cov}_{\text{WMAP9}}^{-1} = \begin{pmatrix} 3.182 & 18.253 & -1.419 \\ 18.253 & 11887.879 & -193.808 \\ -1.429 & -193.808 & 4.556 \end{pmatrix}. \quad (37)$$

On the other hand, for a flat w CDM, Neveu et al. (2016) estimated from Planck measurements: $l_A^{obs} = 301.787 \pm 0.089$, $R^{obs} = 1.7492 \pm 0.0049$, $z_*^{obs} = 1089.99 \pm 0.29$. They also provide the following the inverse covariance matrix, $\text{Cov}_{\text{Pl}}^{-1}$, of these quantities

$$\text{Cov}_{\text{Pl}}^{-1} = \begin{pmatrix} 162.48 & -1529.4 & 2.0688 \\ -1529.4 & 207232 & -2866.8 \\ 2.0688 & -2866.8 & 53.572 \end{pmatrix}. \quad (38)$$

5 RESULTS AND DISCUSSION

In all our estimations, we use Gaussian priors on h (Riess et al. 2016), and $\Omega_b h^2$ (Cooke et al. 2014), which are derived from measurements independent from the CMB and useful in dynamical DE models, thus leaving Ω_m , w_0 , and w_1 ($w_{0.5}$ for the SL model) as the only free parameters of the analysis (see Table 2). To calculate these constraints we assume a Gaussian likelihood $\mathcal{L} \propto \exp(-\chi^2/2)$. First, we obtain the constraints using the measurements of f_{gas} alone. As mentioned before, we consider the $f_{\text{gas}}^{\text{Allen}}$ or the $f_{\text{gas}}^{\text{ACT}}$ sample. We also estimated the parameters from the combination of $H(z)$ +BAO+CMB (WMAP or Planck) and the joint analysis of f_{gas} + $H(z)$ +BAO+CMB. Thus, with the χ^2 functions defined in section §4 for each data, we construct the total χ^2 -function for these three cases: $\chi^2 = \chi_{f_{\text{gas}}}^2$, $\chi^2 = \chi_H^2 + \chi_{\text{BAO}}^2 + \chi_{\text{CMB}}^2$, and $\chi^2 = \chi_{f_{\text{gas}}}^2 + \chi_H^2 + \chi_{\text{BAO}}^2 + \chi_{\text{CMB}}^2$. We perform our Bayesian analysis using the *emcee* Python module (Foreman-Mackey et al. 2013). In all our computations, we consider a total of 6500 steps with 500 walkers and 1000 steps were removed which correspond to the burn-in phase to stabilize the estimations. We start the walkers in a small ball around the expected points of maximum probability estimated with a differential evolution method. To judge the convergence of the sampler we ask that the acceptance fraction is in the $[0.2 - 0.5]$ range and check the autocorrelation time which is found to be $\mathcal{O}(60)$ and $\mathcal{O}(80)$ for the A04 and A08 fitting respectively.

5.1 Impact of f_{gas} fitting function

For all $w(z)$ parameterizations we estimated the cosmological parameters using the chi-squares functions for both A04 and A08 f_{gas} fitting equations. The first one (Eq. 12) assumes that the baryonic fraction from clusters does not depend on redshift, while the second one (Eq. 14) assumes a linear dependence for s and b parameters with redshift. In addition, the A08 equation considers more correction factors due to the underlying cosmological model and the cluster physics. Fig. 1 shows that there is no significant difference in the w_0 and w_1 constraints for the JBP parameterization derived from $f_{\text{gas}}^{\text{Allen}}$ sample when A04 or A08 function are used. When the $f_{\text{gas}}^{\text{ACT}}$ sample is used a similar result is found, and the $q(z)$ parameter trend is the same for both A04 or A08 functions (see Appendix B for more details). In addition, we found the same result for the other $w(z)$ functions. Thus, in what follows, we only present the results obtained using the A04 equation. For completeness, Tables C1-C5 (Tables C4-C5 are available online only) give the best fits for Ω_m , w_0 and w_1 , by considering the A08 fitting function (Eq. 14) in the parameter estimation.

5.2 Impact of f_{gas} measurements on the parameter estimation

Tables and Figures C1-C5 (Tables and Figures C4-C5 are available online only) summarize our results for Ω_m and the EoS parameters for each $w(z)$ parameterization estimated with the different tests. Notice that, in general, the estimations on Ω_m derived from the f_{gas} data are in very good agreement to those obtained from the combination of $H(z)$ +BAO+WMAP and of the joint analysis of the all

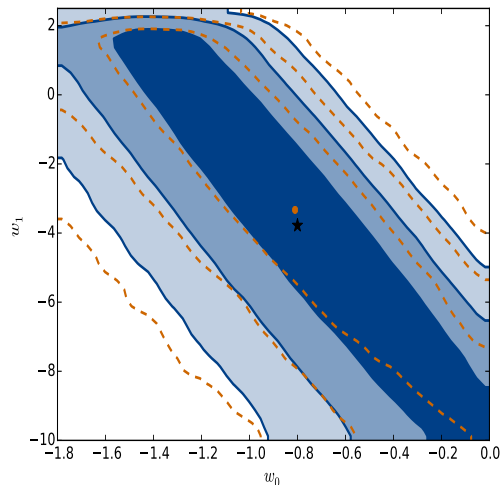


Figure 1. Comparison of the $w_0 - w_1$ confidence contours for the JBP parameterization using the $f_{\text{gas}}^{\text{Allen}}$ data alone with the A04 and A08 equations. The blue filled contours show the 68%, 95% and 99% confidence levels obtained by considering Eq. (12), while the orange dashed contours show the same by considering Eq. (14). The star and the dot marks represent the best fit obtained using each one of these f_{gas} fitting function respectively. Observe that there is no significant statistically difference in the w_0 and w_1 bounds. We found the same result for the other $w(z)$ functions

data sets (see priors in Table 2). Thus we confirm that f_{gas} measurements in galaxy clusters is a suitable probe to put bounds on the content of dark matter in the Universe. For the EoS parameters, w_0 and w_1 , the best fits show different estimations when using f_{gas} , $H(z)$ +BAO+WMAP, and the joint analysis of all data sets. However, these bounds are consistent at the 3σ confidence level (see Fig. 2 for the comparison of the JBP estimations). On the other hand, the bounds estimated with the joint analysis of the data are consistent, at 68% confidence level, with the cosmological constant, i.e., $w_0 \approx -1$ and $w_1 \approx 0$. Since our interest is to focus on the gas mass fraction probe, in what follows, we only present the results obtained using the f_{gas} data and the joint analysis f_{gas} + $H(z)$ +BAO+CMB.

5.3 Cosmic acceleration for the $w(z)$ parameterizations

Tables C1-C5 give the estimated redshift of the transition, z_t , from a decelerated to an accelerated phase. If the slowing down of the CA emerges, we also give the redshift when it occurs. Both redshifts were calculated using the following Monte Carlo approach. We randomly selected a 1:20 subsample of the posterior sample and calculated for each point the $q(z)$ on a grid in z . Then, we obtained the z_t and z_{sd} distributions which are well-approximated by a Gaussian function. Therefore, by producing a histogram, we estimated the central values and its errors. We found that the z_t value estimated using only the $f_{\text{gas}}^{\text{Allen}}$ data is lower than those obtained with the joint analysis of $f_{\text{gas}}^{\text{Allen}}$ + $H(z)$ +BAO+CMB

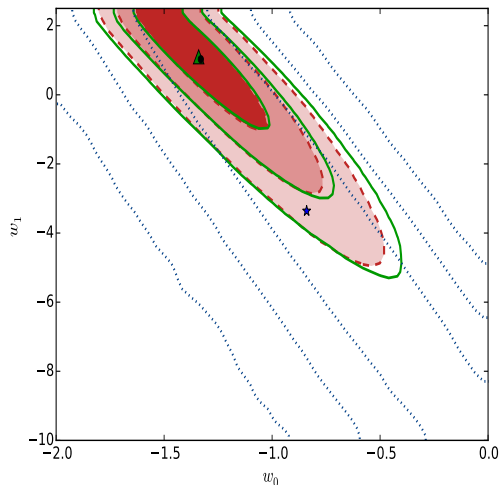


Figure 2. Comparison of the $w_0 - w_1$ 68%, 95% and 99% confidence levels, for the JBP model using $f_{\text{gas}}^{\text{Allen}}$ (no-filled dotted blue contours), $H(z)$ +BAO+WMAP (no-filled green contours), and the joint analysis $f_{\text{gas}}^{\text{Allen}} + H(z)$ +BAO+WMAP (filled dashed red contours) data. The star, triangle, and dot represent the best fit obtained using each one of these data set respectively. The best fit obtained using f_{gas} is consistent at 3σ level with those obtained from $H(z)$ +BAO+WMAP and the joint analysis.

data. We reconstructed the cosmological evolution of the $q(z)$ parameter and propagated its error as follows. By considering the subsample, we produced a well-approximated Gaussian distribution of $q(z_i)$ for each z_i on the grid in z and determined the central value, 1 and 2σ levels. The behaviour of the $q(z)$ parameter for each parameterization using the $f_{\text{gas}}^{\text{Allen}}$, $H(z)$ +BAO+WMAP, and the joint analysis of $f_{\text{gas}}^{\text{Allen}} + H(z)$ +BAO+WMAP data are shown in the left panel of Figure 3. We found that for all parameterizations (except for FSLII, which presents a behavior slightly oscillatory) the CA has two transitions when the f_{gas} constraints are used. At redshifts $0.67 < z_t < 0.72$, the Universe begins its accelerated expansion, however, it reaches a peak of acceleration at $0.19 < z_{sd} < 0.24$ and then the acceleration slows down. Moreover, this trend is supported at 2σ confidence level (dashed lines in Fig. 3). Our results are in good agreement with those obtained by Wang et al. (2015). They found that in the JBP, BA and FSLI parameterizations the cosmic acceleration presents a slowing down at $z \sim 0.24, 0.26$, and 0.28 respectively within the 2σ confidence level. Nevertheless, we calculated the Akaike information criteria (AIC, Akaike 1974) and Bayesian information criteria (BIC, Schwarz 1978) for the Λ CDM and the five dynamical DE models. By comparing with the Λ CDM, we obtained that the dynamical models lead larger AICs (~ 3) and BICs (~ 12) values, indicating that a dynamical DE model is not necessary to explain the f_{gas} data. (this result is similar to that obtained by Wang et al. 2015). Since that the slowing down of cosmic acceleration depend on the $w_0 - w_1$ values, which are completely degenerated, it is crucial to provide narrow EoS constraints to prevent misleading

results. A future increase in f_{gas} points (i.e. decrease in the systematic uncertainties) will produce a better parameter estimation for $w(z)$ parameterizations. For instance, Mantz et al. (2014) simulated the f_{gas} measurements for 400 galaxy clusters and obtained for an evolving DE model an increase in the Figure-of-Merit (FoM) by a factor ~ 15 in an optimistic scenario of future surveys (this implies a reduction of the area enclosed by the $w_0 - w_1$ 95% confidence contour and the EoS constraints are very close to the cosmological constant). Therefore the slowing down of cosmic acceleration obtained from f_{gas} constraints could be only a statistical fluctuation.

On the other hand, if the $H(z)$ +BAO+WMAP constraints are used to reconstruct $q(z)$, we found that it evolves similarly to that of the cosmological constant. When we used the estimations obtained with the joint analysis of the all data, the transition from a decelerated to an accelerated phase occurs at $0.64 < z_t < 0.70$ and $q(z) \sim -0.7$ at $z \rightarrow 0$, i.e., the slowing down of the CA disappears, and it evolves as the cosmological constant. Furthermore, we found that the evolution of the CA is independent of the EoS parameterization (see the different panels of Fig. 3). This same scenario was found by Magaña, Cárdenas & Motta (2014) when several SNIa data sets are considered (see also Wang et al. 2015; Shi et al. 2011). Although to discern which model is the preferred one by observations is not the scope of this paper, it can be determined by comparing the χ_{min} , given in Tables C1-C5, among data sets. Any $w(z)$ parametrization could be plausible to model a dynamical dark energy.

5.4 Impact of CMB data on $q(z)$

As shown in the previous section, when the CMB data from WMAP measurements are included, the slowing down of the CA, which emerges when only low-redshift data are used, disappears (see also Shafieloo, Sahni & Starobinsky 2009; Li, Wu & Yu 2011; Cárdenas & Rivera 2012; Cárdenas, Bernal & Bonilla 2013; Magaña, Cárdenas & Motta 2014). Nevertheless, in a recent paper, Wang et al. (2015) found that for the CPL parameterization, when the Planck data (from the 2013 and 2015 measurements, Planck collaboration 2013, 2015,b) in combination with the BAO and SNIa (JLA sample) data are considered in the analysis, the slowing down of the CA is still present at the 1σ and 2σ levels. To prove this result, we also consider the Planck 2015 data in the f_{gas} and $f_{\text{gas}} + H(z)$ +BAO+CMB analysis. We found that there are no significative differences between the best fits on Ω_m obtained using Planck with those from WMAP (see tables C1-C5 and Figures C1-C5). Additionally, the w_0 and w_1 constraints obtained using Planck data in the joint analysis are consistent at 1σ confidence level to those estimated including WMAP measurements. When $q(z)$ is reconstructed for each parameterization using the constraints derived of the combination of all data, we obtain that the universe evolves from a decelerated phase to one accelerated phase at $0.63 < z_t < 0.68$, and at $z \rightarrow 0$ the cosmic acceleration is consistent with that of the standard model (see right panels of Fig. 3). This result is in agreement with those obtained using WMAP data where the slowing down of CA obtained using the gas mass fraction disappears by adding the CMB (high-redshift) information. Nevertheless, our result is in tension with that found by Wang et al. (2015) and

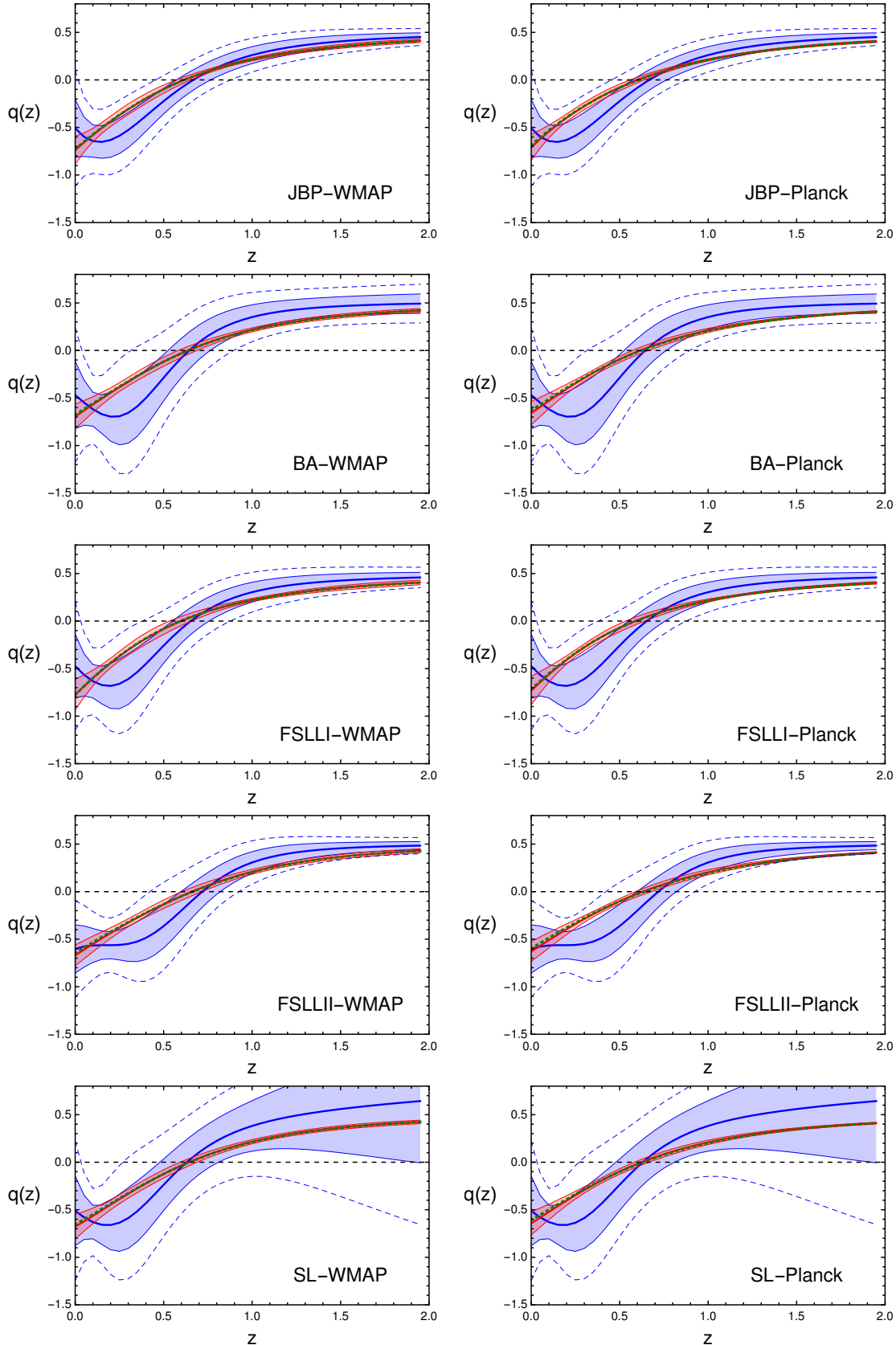


Figure 3. Reconstructed $q(z)$ deceleration parameter for each $w(z)$ parameterization: from the top to bottom panels, JBP, BA, FSLLI, FSLLI, and SL parameterizations respectively. The left and right show the results obtained using WMAP and Planck data respectively. The $q(z)$ computed from the $f_{\text{gas}}^{\text{Allen}}$ constraints is shown in blue solid line. The result obtained from the $f_{\text{gas}}^{\text{Allen}} + H(z) + \text{BAO} + \text{CMB}$ limits is shown in red solid line. The shadow (dashed lines) regions show the 1σ (2σ) region calculated with the error propagation for each data set. For completeness, the dotted green line shows the reconstructed $q(z)$ using the $H(z) + \text{BAO} + \text{CMB}$ limits.

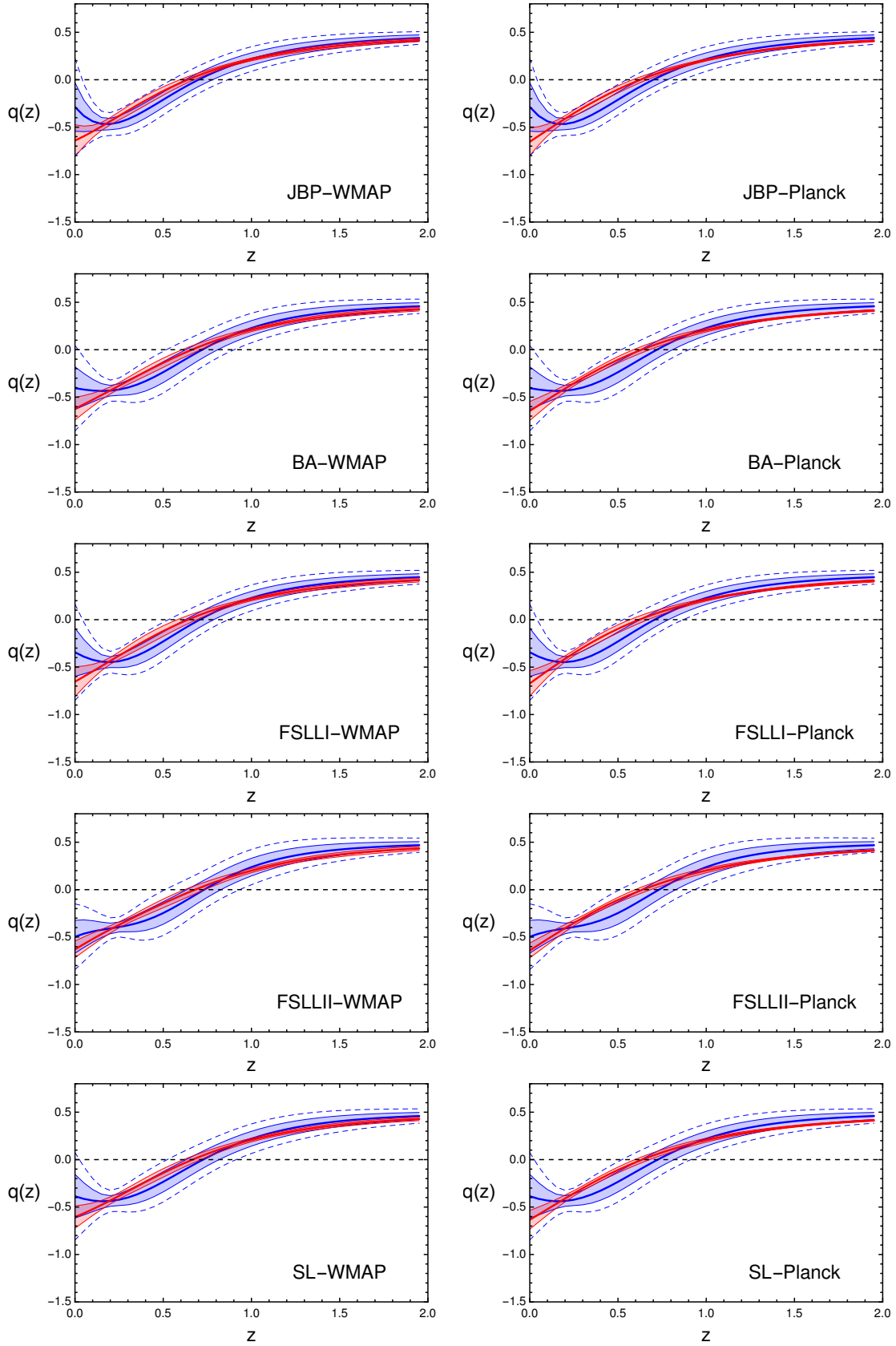


Figure 4. Reconstructed $q(z)$ deceleration parameter for each $w(z)$ parameterization: from the top to bottom panels, JBP, BA, FSLLI, FSLLI, and SL parameterizations respectively. The left and right show the results obtained using WMAP and Planck data respectively. The $q(z)$ computed from the $f_{\text{gas}}^{\text{ACT}}$ constraints is shown in blue solid line. The result obtained from the $f_{\text{gas}}^{\text{ACT}} + H(z) + \text{BAO} + \text{CMB}$ limits is shown in red solid line. The shadow (dashed lines) regions show the 1σ (2σ) region calculated with the error propagation.

we check that the Planck 2015 measurements do not favor a slowing down of the CA.

5.5 Impact of the $f_{\text{gas}}^{\text{ACT}}$ sample on the constraints

In the previous sections, we have presented the results using the $f_{\text{gas}}^{\text{Allen}}$ in the $w(z)$ fitting. Here we investigate whether the slowing down of the CA appears when the $f_{\text{gas}}^{\text{ACT}}$ sample, with about twice the data points by $f_{\text{gas}}^{\text{Allen}}$ set, is used in the parameter estimation. As before, we estimate the Ω_m , w_0 , and w_1 constraints using only the f_{gas} data and the joint analysis $f_{\text{gas}} + H(z)$ +BAO+CMB (WMAP or Planck). We give the best fits for each parameterization in Tables C1-C5. Notice that the Ω_m constraints from the different data sets are very similar to those obtained when the $f_{\text{gas}}^{\text{Allen}}$ sample was used. Although there is a slightly tension in the w_0 and w_1 best fits obtained from both gas mass fraction samples, they are consistent within their 68% confidence regions. When the $q(z)$ deceleration parameter for each $w(z)$ is reconstructed using the $f_{\text{gas}}^{\text{ACT}}$ constraints, the transition from a decelerated phase to an accelerated phase occurs at $\simeq 0.75$. We also found that the $f_{\text{gas}}^{\text{ACT}}$ is consistent at the 2σ confidence level with the slowing down of the CA at $0.20 < z_{sd} < 0.25$ for the JBP, BA, FSLII, and SL parameterizations (see left panels of Fig. 4). Notice that this trend is softened compared with those obtained using the $f_{\text{gas}}^{\text{Allen}}$ sample. As in the case of SNIa data, we confirm that this trend occurs for several f_{gas} samples. By reconstructing $q(z)$ using the $f_{\text{gas}}^{\text{ACT}} + H(z)$ +BAO+WMAP (Planck) constraints, the CA evolves as the cosmological constant and the Universe passes from a decelerated phase to an accelerated phase at $0.68 < z_t < 0.72$ ($0.66 < z_t < 0.69$). It is worth to note that the $f_{\text{gas}}^{\text{ACT}}$ sample could yield biased constraints due to the cluster gas physics and underlying cosmology assumed in the $f_{\text{gas}} - M_{500}$ relation (Eq. 17) which was used to compute the data point. To take into account its bias we performed a test using large f_{gas} uncertainties (see Appendix A) and we found no significative differences on the Ω_m , w_0 , and w_1 constraints, leading to similar evolutions of $q(z)$ as those obtained with normal errors.

6 CONCLUSIONS

We investigated the evolution of the deceleration parameter $q(z)$ in the following models with the EoS as a function of redshift using gas mass fraction measurements in galaxy clusters: JBP, BA, FSLII, FSLIII, and SL. We used two f_{gas} data sets: the sample by Allen et al. (2004) which consists of 42 points spanning the redshift range $0.05 < z < 1.1$ and the ACT sample which consists of 91 data points in the redshift range $0.118 < z < 1.36$ (Hasselfield et al. 2013). These $f_{\text{gas}}^{\text{ACT}}$ data points were computed using a $f_{\text{gas}} - M_{500}$ relation (Vikhlinin et al. 2009). In spite of the difference between the samples, they both provide consistent estimations for the cosmological parameters. We validated that the gas mass fraction test is a qualified tool to constrain the cosmological parameters Ω_m , w_0 , w_1 , and then the CA in these models.

We also considered different fitting function for the f_{gas} data points: A04 (Eq. 12) and A08 (Eq. 14). The main difference between both functions is that the second one considers

several corrections due to the underlying cosmology and the cluster physics. We found that the A08 fitting function does not offer significantly better cosmological constraints than the simplest A04 function (see Fig.1).

A MCMC analysis was performed using the f_{gas} data and the joint $f_{\text{gas}} + H(z)$ +BAO+CMB (WMAP and Planck) measurements. We used these data sets to reconstruct the $q(z)$ parameter. For all parameterizations (except for FSLIII), a slowing down of CA emerges at late times (at the 2σ confidence level) when using the f_{gas} data alone, i.e. different $w(z)$ functions does not influence the $q(z)$ cosmic evolution. This is in agreement with results obtained by Magaña, Cárdenas & Motta (2014, see also Shi et al. 2011) using several SNIa samples. Our results are also in agreement with those obtained by Wang et al. (2015), who performed a comprehensive analysis with several cosmological data. Furthermore, our results suggest that this CA trend is not a systematic effect produced by SNIa or f_{gas} samples (as suggested previously by Shafieloo, Sahni & Starobinsky (2009); Cárdenas, Bernal & Bonilla (2013); Magaña, Cárdenas & Motta (2014); Wang et al. (2015)). Nevertheless, the emergence of the slowing down of cosmic acceleration depend on the $w_0 - w_1$ values. Therefore, to prevent misleading results, it is crucial to provide narrow EoS constraints. Here, we used two f_{gas} samples, by Allen and ACT, which have poor statistics. A future increase in f_{gas} points (i.e. decrease in the systematic uncertainties) will produce a better parameter estimation for $w(z)$ parameterizations. For instance, Mantz et al. (2014) simulated the f_{gas} measurements for 400 galaxy clusters and obtained for an evolving DE model an increase in the FoM by a factor ~ 15 in an optimistic scenario of future surveys (this implies a reduction of the area enclosed by the $w_0 - w_1$ 95% confidence contour and the EoS constraints are very close to the cosmological constant). Therefore the slowing down of cosmic acceleration obtained from f_{gas} constraints could be only a statistical fluctuation.

On the other hand, the CA behavior changes when the $H(z)$ +BAO+CMB constraints are used. We obtained for each parameterization that these data favor an accelerated expansion at late times. The $q(z)$ reconstructed from the joint analysis $f_{\text{gas}} + H(z)$ +BAO+CMB (WMAP and Planck) shows that the CA behaves as the cosmological constant. Our result is in tension with those obtained by Wang et al. (2015), who found a CA slowing down for the CPL parameterization using the Planck data.

We investigated the impact to consider the $f_{\text{gas}}^{\text{ACT}}$ sample and we confirmed that, in general, it is consistent at the 2σ confidence level with the slowing down CA (except for the FSLIII parameterization). As in the $f_{\text{gas}}^{\text{Allen}}$ case, this trend disappears by adding the $H(z)$, BAO and WMAP measurements in the parameter estimation.

Finally, our results suggest that several low-redshift cosmological data are consistent with a CA slowing down when $w(z)$ is parameterized. Although this trend does not emerge in other approaches to study the evolution of $q(z)$ (see for example Rani et al. 2015; Zhang & Xia 2016) we encourage to the community to further investigate this phenomena in DE models. To improve our constraints, a large high precision f_{gas} sample is needed.

7 ACKNOWLEDGMENTS

We thank the anonymous referee for thoughtful remarks and suggestions. J.M. acknowledges support from Gemini 32130024 and FONDECYT 3160674. V.M. acknowledges support from ECOS-CONICYT C12U02 and Centro de Astrofísica de Valparaíso. V.C. acknowledges support from DIUV 50/2013,

REFERENCES

- Akaike, H. 1974, ITAC, 19, 716
 Albrecht et al., 2006, Report of the Dark Energy Task Force, arXiv:astro-ph/0609591
 Allen S.W., Schmidt R.W., Ebeling H., Fabian A.C. and Speybroeck L. van, 2004, MNRAS 353, 457.
 Allen S.A., Rapetti D.A., Schmidt R.W., Ebeling H., Morris G. and Fabian A.C., 2008, MNRAS 383, 879.
 Amanullah R. et al., 2010, ApJ 716, 712
 Anderson L., Aubourg E., Bailey S., et al., 2014, MNRAS, 439, 83.
 Anderson L., Aubourg E., Bailey S., Beutler, F., Bhardwaj, V., et al., 2014, MNRAS, 441, 24.
 Anderson L., Aubourg E., Bailey S., et al., 2012, MNRAS, 427, 3435.
 Barboza E. M. Jr. and Alcaniz J. S., 2008, PLB, 666, 415.
 Beutler F., Blake C., Colless M., et al., 2011, MNRAS, 416, 3017.
 Betoule, M., Kessler, R., Guy, J., Mosher, J., Hardin, D., et al., 2014, A&A, 568, A22
 Blake C., Kazin E. A., Beutler F., et al., 2011, MNRAS, 418, 1707.
 Blake C., Brough S., Colless M., et al., 2012, MNRAS, 425, 405.
 Bonamente M., Joy M. K., LaRoque S. J., Carlstrom J. E., Reese E. D., Dawson K. S., 2006, ApJ, 647, 25.
 Bond J. R., Efstathiou G., Tegmark M., 1997, MNRAS, 291, L33.
 Busca N. G., Delubac T., Rich J., et al., 2013, A&A 552, 18.
 Cárdenas V. H., Rivera M., 2012, PLB, 710, 251.
 Cárdenas V. H., Bernal C., Bonilla A., 2013, MNRAS, 433, 3534
 Chen Y., Geng C.-Q., Cao S., H. Y.-M., Zhu Z.-H., 2013, arXiv:1312.1443.
 Chevallier M., Polarski D., 2001, IJMPD, 10, 213.
 Chuang C.-H., and Wang Y., 2013, MNRAS, 435, 255.
 Cooke, R. J., Pettini, M., Jorgenson, R. A., Murphy, M. T., Steidel, C. C. et al. 2014, ApJ, 781, 31
 Conley, A., Guy, J., Sullivan, M., et al. 2011, ApJS, 192, 1
 Copeland E. J., Sami M., Tsujikawa S., 2006, IJMPD, 15, 1753,
 D'Agostini, G., 2004, arXiv:physics/0403086.
 Davis, T. M., 2014, GReGr, 46, 1731
 Delubac T., Bautista J. E., Busca N. G., et al., 2015, A&A, 574, A59
 Di Valentino E., Melchiorri A. and Silk J., 2015, PRD, 92, 121302.
 Eisenstein D. J. and Hu W., 1998, ApJ, 496, 605.
 Eisenstein D. J. et al., 2005, ApJ, 633, 560.
 Ettori S., Morandi A., Tozzi P., et al., 2009, A&A 501, 61.
 Farooq O., and Ratra B., 2013, ApJ, 766, L7.
 Feng C. -J., Shen X. -Y., Li P. and Li X. -Z., 2012, JCAP, 209, 023.
 Font-Ribera, A., Kirkby, D., Busca, N., Miralda-Escudé, J., Ross, N. P., et al., 2014, JCAP, 05, 027
 Foreman-Mackey, D., Hogg, D. W., Lang, D., Goodman, J., 2013, PASP, 125, 306
 Ganeshalingam M., Li W. and Filippenko A. V., 2013, MNRAS 433, 2240.
 Gaztañaga E., Cabré A., and Hui L., 2009, MNRAS, 399, 1663.
 Gonçalves R. S., Bernui A., Holanda R. F. L., Alcaniz J. S., 2015, A&A, 573, A88
 Gong, Y., Gao, Q., Zhu, Z.-H., 2013, MNRAS, 430, 3142
 Gong, Y., Ma, Y.-Z., Zhang, S.-N., Chen, X., 2015, PRD, 92, 063523.
 Guimarães, A.C.C., Lima, J.A.S., 2011, CQG, 28, 125026
 Hasselfield M., Hilton M., Marriage T. A., et al., 2013, JCAP, 07, 008.
 Hicken, M., Wood-Vasey, W. M., Blondin, S., Challis, P., Jha, S., et al., 2009, ApJ, 700, 1097
 Hinshaw G., et al., 2013, ApJS, 208, 19.
 Hu W. and Sugiyama N., 1996, ApJ, 471, 542.
 Jassal H. K., Bagla J. S., and Padmanabhan T., 2005, MNRAS, 356, L11.
 Jassal H. K., Bagla J. S., and Padmanabhan T., 2005, PRD, 72, 103503.
 Joyce, A., Lombriser, L., & Schmidt, F. 2016, arXiv:1601.06133
 Kazin, E. A., Koda, J., Blake, C., Padmanabhan, N., Brough, S., et al., 2014, MNRAS, 441, 3524
 Komatsu, E., et al., 2009, ApJS, 180, 330
 Komatsu, E., et al., 2011, ApJS, 192, 18
 LaRoque S. J., Bonamente M., Carlstrom J. E., et al., 2006, ApJ 652, 917.
 Li, H., Xia, J.-Q., Zhao, G.-B., Fan, Z., and Zhang, X., 2008, ApJ, 683, L1
 Li Z., Wu P., Yu H., 2011, PLB, 695, 1.
 Li, M., Li, X.-D., Wang, S., Wang, Y., 2013, Frontiers of Physics, 8, 828
 Linder E. V., 2003, PRL, 90, 091301.
 Magaña J., Cárdenas V. H., Motta V., 2014, JCAP, 10, 017
 Magaña J., Motta V., Cárdenas V. H., Verdugo, T., Jullo, E., 2015, ApJ, 813, 69
 Mantz A. B., Allen S. W., Morris R. G., et al., 2014, MNRAS, 440, 2077.
 Marra V., Amendola L., Sawicki I. and Valkenburg W., 2013, PRL, 110, 24, 241305
 Moresco M., Cimatti M., Jimenez R., et al., 2012, JCAP, 08, 006.
 Mortonson, M. J.; Weinberg, D. H., White, M., 2014, Chapter 25 of Particle Data Group 2014 Review of Particle Physics, arXiv:1401.0046.
 Mukherjee, P., Kunz, M., Parkinson, D., & Wang, Y., 2008, PRD 78, 083529
 Nesseris S. and Perivolaropoulos L., 2007, JCAP 01, 018.
 Neveu, J., Ruhlmann-Kleider, V., Astier, P., Besançon, M., Guy, J., et al., 2016, arXiv:1605.02627
 Oka, A., Saito, S., Nishimichi, T., Taruya, A., and Yamamoto, K., 2014, MNRAS, 439, 2515
 Percival W. J., et al., 2010, MNRAS, 401, 2148.
 Perlmutter, S., Aldering, G., Goldhaber, G., Knop, R. A.,

- Nugent, P., et al., 1999, ApJ, 517, 565
- Planck collaboration: Ade P. A. R., et al., 2014, A & A, 571, A16
- Planck collaboration: Ade P. A. R., et al., 2015, arXiv:1502.01589
- Planck collaboration: Ade P. A. R., et al., 2015, arXiv:1502.01590
- Rani, N., Jain, D., Mahajan, S., Mukherjee, A., Pires, N., 2015, JCAP, 12, 045
- Riess, A. G., Filippenko, A. V.; Challis, P., Clocchiatti, A., Diercks, A., et al., AJ, 116, 1009
- Riess, A. G., Macri, L. M., Hoffmann, S. L., Scolnic, D., Casertano, et al., 2016, Accepted in ApJ, arXiv:1604.01424
- Ross, A. J.; Samushia, L., Howlett, C., Percival, W. J., Burden, et al., 2015, MNRAS, 449, 835
- Sasaki S., 1996, PASJ, 48, L119.
- Sendra I., and Lazkoz R., 2012, MNRAS, 422, 776.
- Shafieloo A., Sahni V. and Starobinsky A.A., 2009, PRD 80, 101301
- Sharov, G. S. and Vorontsova, E. G., 2014, JCAP, 10, 057
- Shi, K., Huang, Y.-F., Lu, T., 2011, RAA, 11, 1403
- Stern D., Jimenez R., Verde L., Kamionkowski M., and Stanford S. A., 2010, JCAP, 02, 008.
- Susuki, N., Rubin, D., Lidman, C., Aldering, G., Amanullah, R. *et al.*, 2012, ApJ 746, 85.
- Schwarz, G. 1978, AnSta, 6, 461
- Vikhlinin A., 2009, ApJ, 692, 1033.
- Wang Y., Mukherjee P., 2006, ApJ, 650, 1
- Wang, Y., Chuang, C.-H-, Mukherjee, P., 2012, PRD, 85, 023517
- Wang, S., Hu, Y., Li, M., Li, N., 2016, ApJ, 821, 60.
- Weinberg S., 1989, RMP, 61, 1.
- Wetterich C., 1988, Nucl. Phys. B, 302, 668.
- Wright, E. L., 2007, ApJ, 664, 633
- Zhang C., Zhang H., Yuan S., Zhang T.-J. and Sun Y.-C., 2014, RAA, 14, 1221
- Zhang M.-J. and Xia J.-Q., 2016, JCAP, 12, 005

APPENDIX B: IMPACT OF THE A08 FITTING FUNCTION WHEN THE $f_{\text{gas}}^{\text{ACT}}$ IS USED

To test whether the constraints derived from the $f_{\text{gas}}^{\text{ACT}}$ sample are improved using the A08 fitting function instead of the A04 we constrain the JBP model using both fitting functions. The left panel of the Fig. B1 shows that there is no significant difference in the w_0 and w_1 constraints when A04 or A08 functions are used. In addition, the right panel of the Fig. B1 shows that the $q(z)$ parameter behaviour is essentially the same when the best fits derived from both functions are used. We found the same result for the other $w(z)$ functions.

APPENDIX C: TABLES AND CONFIDENCE CONTOURS FOR EACH MODEL USING f_{gas} AND $f_{\text{gas}}+H(Z)+\text{BAO}+\text{CMB}$

APPENDIX D: THE H(Z) DATA SET

APPENDIX A: IMPACT OF THE UNCERTAINTIES ON THE $f_{\text{gas}} - M_{500}$ RELATION

The cosmological constraints in the models could be biased due to the uncertainties on the scaling relation parameters in the Eq. 17. To test the impact of these uncertainties, we constrain, for instance, the JBP model using 15% error in each parameter of the equation. Figure A1 shows that the best fit using 15% errors is within the 1σ confidence level of the previous best fit (see Figure C1). Figure A1 also shows that the $q(z)$ parameter exhibits the slowing down feature at 1σ level as presented before (Figure 3). The scatter in the $f_{\text{gas}} - M_{500}$ scaling relation has little or no significant impact in the cosmological parameter estimation up to 1σ confidence level.

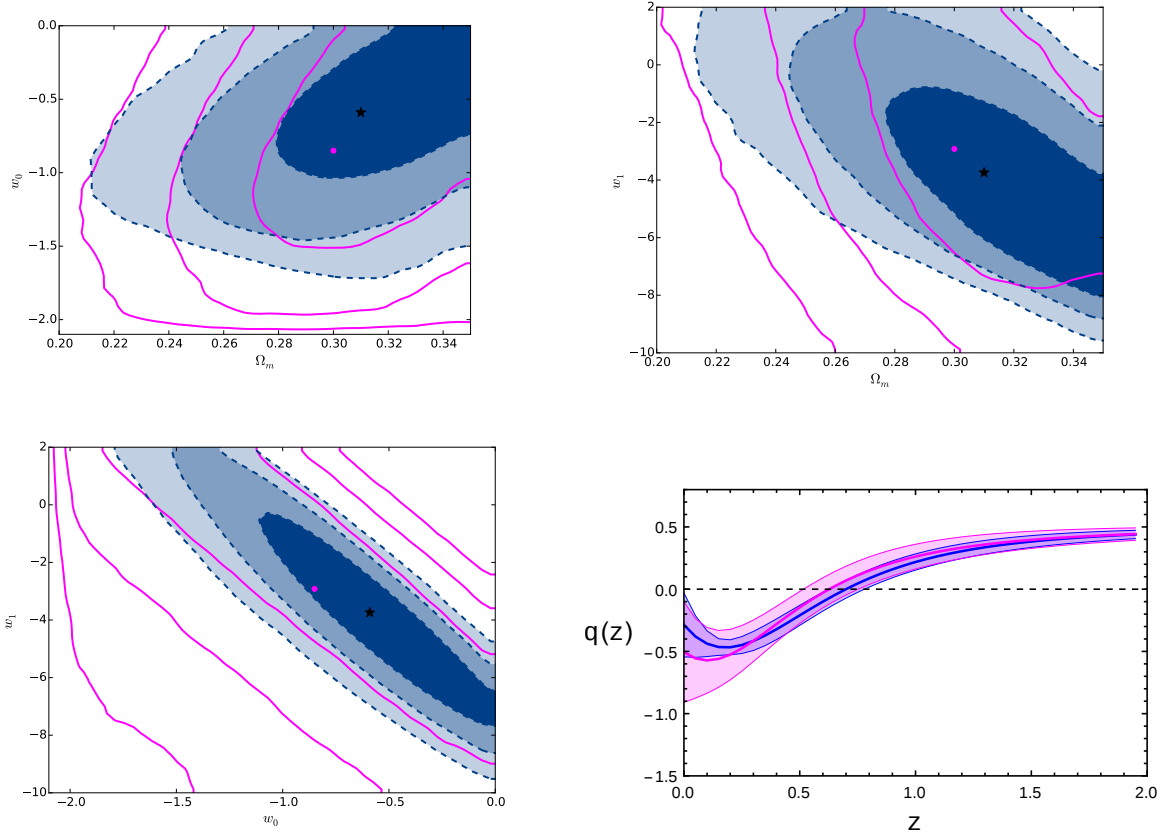


Figure A1. The top panels and the bottom left panel show the 2D at 68%, 95%, 99% confidence levels for the Ω_m , w_0 , and w_1 parameters of the JBP parameterization obtained from the $f_{\text{gas}}^{\text{ACT}}$ data alone for two cases: using the best fit values of the $f_{\text{gas}} - M_{500}$ scaling relation (blue filled contours) and using 15% error in each parameter of the equation (magenta no-filled contours). The star and dot marks represent the best value obtained using each one of these cases respectively. The bottom right panel shows the reconstructed $q(z)$ parameter for these two cases. We found that a 15% scatter in the $f_{\text{gas}} - M_{500}$ scaling relation has little or no significant impact in the cosmological parameter estimation up to 1σ confidence level.

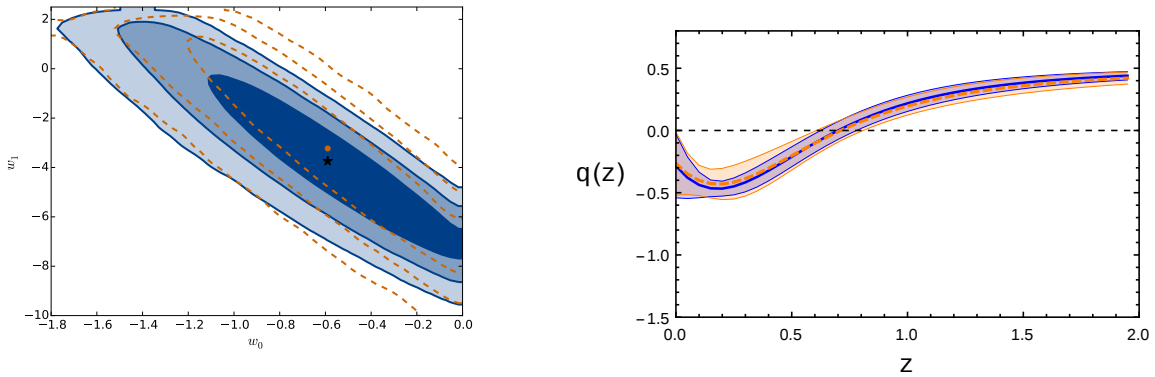


Figure B1. The left panel shows the $w_0 - w_1$ 68%, 95%, 99% confidence levels for the JBP parameterization obtained from the $f_{\text{gas}}^{\text{ACT}}$ data alone using the A04 (blue filled contours) and A08 (orange no-filled contours) fitting functions. The star and dot marks represent the best value obtained using each one of these functions respectively. The right panel shows the reconstructed $q(z)$ parameter using these two cases: A04 (blue solid line) and A08 (orange dashed line). The shadow regions show the 1σ region calculated with the error propagation of the cosmological parameters. We found that the $q(z)$ parameter behaviour is essentially the same when the best fits derived from both functions are used.

JBP parameterization						
Data set	χ_{min}^2	Ω_m	w_0	w_1	z_t	z_{sd}
H(z)+BAO+W9	49.32	$0.28^{+0.01}_{-0.01}$	$-1.25^{+0.22}_{-0.16}$	$0.51^{+0.99}_{-1.47}$	$0.66^{+0.04}_{-0.04}$	No
H(z)+BAO+P1	67.22	$0.29^{+0.01}_{-0.01}$	$-1.22^{+0.21}_{-0.16}$	$0.55^{+0.91}_{-1.18}$	$0.65^{+0.04}_{-0.04}$	No
A04						
f_{gas}^{Allen}	41.80	$0.28^{+0.03}_{-0.03}$	$-0.80^{+0.45}_{-0.45}$	$-3.78^{+3.73}_{-3.76}$	$0.71^{+0.09}_{-0.09}$	$0.20^{+0.06}_{-0.09}$ (2.6)
f_{gas}^{ACT}	160.71	$0.31^{+0.02}_{-0.03}$	$-0.59^{+0.34}_{-0.39}$	$-3.74^{+2.50}_{-2.19}$	$0.75^{+0.08}_{-0.07}$	$0.23^{+0.05}_{-0.09}$ (3.2)
f_{gas}^{Allen} +H(z)+BAO+W9	91.40	$0.28^{+0.01}_{-0.01}$	$-1.26^{+0.21}_{-0.15}$	$0.53^{+0.97}_{-1.41}$	$0.66^{+0.04}_{-0.04}$	No
f_{gas}^{Allen} +H(z)+BAO+P1	109.29	$0.29^{+0.01}_{-0.01}$	$-1.24^{+0.19}_{-0.15}$	$0.65^{+0.85}_{-1.08}$	$0.64^{+0.04}_{-0.03}$	No
f_{gas}^{ACT} +H(z)+BAO+W9	212.64	$0.29^{+0.01}_{-0.01}$	$-1.12^{+0.23}_{-0.20}$	$-0.31^{+1.30}_{-1.53}$	$0.68^{+0.03}_{-0.04}$	No
f_{gas}^{ACT} +H(z)+BAO+P1	231.30	$0.29^{+0.01}_{-0.01}$	$-1.15^{+0.20}_{-0.18}$	$0.05^{+1.05}_{-1.17}$	$0.67^{+0.04}_{-0.04}$	No
A08						
f_{gas}^{Allen}	41.93	$0.29^{+0.03}_{-0.04}$	$-0.81^{+0.47}_{-0.48}$	$-3.33^{+3.44}_{-3.69}$	$0.71^{+0.13}_{-0.11}$	$0.20^{+0.07}_{-0.10}$ (2.3)
f_{gas}^{ACT}	174.41	$0.31^{+0.02}_{-0.03}$	$-0.59^{+0.36}_{-0.40}$	$-3.23^{+2.93}_{-2.76}$	$0.75^{+0.10}_{-0.10}$	$0.24^{+0.05}_{-0.10}$ (3.2)
f_{gas}^{Allen} +H(z)+BAO+W9	91.32	$0.28^{+0.01}_{-0.01}$	$-1.24^{+0.21}_{-0.16}$	$0.44^{+1.03}_{-1.42}$	$0.66^{+0.04}_{-0.04}$	No
f_{gas}^{Allen} +H(z)+BAO+P1	109.01	$0.29^{+0.01}_{-0.01}$	$-1.22^{+0.19}_{-0.16}$	$0.54^{+0.90}_{-1.12}$	$0.65^{+0.04}_{-0.04}$	No
f_{gas}^{ACT} +H(z)+BAO+W9	212.44	$0.29^{+0.01}_{-0.01}$	$-1.12^{+0.23}_{-0.19}$	$-0.11^{+1.25}_{-1.58}$	$0.67^{+0.04}_{-0.04}$	No
f_{gas}^{ACT} +H(z)+BAO+P1	231.08	$0.29^{+0.01}_{-0.01}$	$-1.11^{+0.20}_{-0.18}$	$0.00^{+1.04}_{-1.17}$	$0.66^{+0.04}_{-0.04}$	No

Table C1. Best fits for the Ω_m , w_0 , and w_1 parameters using two f_{gas} fitting functions (A04 and A08) and several data sets for the JBP parameterization. We also present the estimated transition redshift, z_t , when the Universe changes from a decelerated to an accelerated phase. If the slowing down of the CA emerges, we also give the redshift, z_{sd} , when it occurs. In parenthesis we also give the distance between zero and z_{sd} in units of standard deviation. It is worth to note that we report asymmetric errors in our estimations and then we consider the D'Agostini criteria (D'Agostini 2004) to obtain $\sigma_{z_{sd}} = (\sigma_{z_{sd}}^+ + \sigma_{z_{sd}}^-)/2$.

BA parameterization						
Data set	χ_{min}^2	Ω_m	w_0	w_1	z_t	z_{sd}
H(z)+BAO+W9	49.85	$0.28^{+0.01}_{-0.01}$	$-1.16^{+0.14}_{-0.14}$	$-0.04^{+0.30}_{-0.37}$	$0.68^{+0.05}_{-0.05}$	No
H(z)+BAO+P1	67.46	$0.29^{+0.01}_{-0.01}$	$-1.12^{+0.13}_{-0.13}$	$0.007^{+0.22}_{-0.24}$	$0.67^{+0.05}_{-0.04}$	No
A04						
f_{gas}^{Allen}	41.71	$0.28^{+0.03}_{-0.03}$	$-0.80^{+0.48}_{-0.59}$	$-2.18^{+2.32}_{-2.54}$	$0.68^{+0.11}_{-0.12}$	$0.19^{+0.06}_{-0.09}$ (2.5)
f_{gas}^{ACT}	161.52	$0.31^{+0.02}_{-0.02}$	$-0.85^{+0.25}_{-0.25}$	$-1.07^{+0.79}_{-0.83}$	$0.75^{+0.08}_{-0.09}$	$0.20^{+0.06}_{-0.10}$ (2.5)
f_{gas}^{Allen} +H(z)+BAO+W9	91.92	$0.28^{+0.01}_{-0.01}$	$-1.17^{+0.13}_{-0.12}$	$-0.03^{+0.28}_{-0.35}$	$0.68^{+0.05}_{-0.05}$	No
f_{gas}^{Allen} +H(z)+BAO+P1	109.78	$0.29^{+0.01}_{-0.01}$	$-1.15^{+0.12}_{-0.11}$	$0.04^{+0.20}_{-0.22}$	$0.66^{+0.04}_{-0.04}$	No
f_{gas}^{ACT} +H(z)+BAO+W9	212.49	$0.29^{+0.01}_{-0.01}$	$-1.10^{+0.12}_{-0.11}$	$-0.20^{+0.30}_{-0.37}$	$0.70^{+0.05}_{-0.05}$	No
f_{gas}^{ACT} +H(z)+BAO+P1	231.30	$0.29^{+0.008}_{-0.008}$	$-1.13^{+0.10}_{-0.10}$	$-0.02^{+0.20}_{-0.22}$	$0.68^{+0.04}_{-0.04}$	No
A08						
f_{gas}^{Allen}	41.85	$0.29^{+0.03}_{-0.04}$	$-0.86^{+0.48}_{-0.49}$	$-1.72^{+1.98}_{-2.31}$	$0.67^{+0.14}_{-0.16}$	$0.18^{+0.07}_{-0.09}$ (2.2)
f_{gas}^{ACT}	174.33	$0.31^{+0.02}_{-0.03}$	$-0.83^{+0.29}_{-0.26}$	$-0.92^{+1.01}_{-1.28}$	$0.73^{+0.10}_{-0.15}$	$0.19^{+0.06}_{-0.12}$ (2.1)
f_{gas}^{Allen} +H(z)+BAO+W9	91.75	$0.28^{+0.01}_{-0.01}$	$-1.16^{+0.13}_{-0.13}$	$-0.06^{+0.29}_{-0.36}$	$0.68^{+0.05}_{-0.05}$	No
f_{gas}^{Allen} +H(z)+BAO+P1	109.39	$0.29^{+0.01}_{-0.01}$	$-1.13^{+0.12}_{-0.12}$	$0.01^{+0.21}_{-0.23}$	$0.67^{+0.04}_{-0.04}$	No
f_{gas}^{ACT} +H(z)+BAO+W9	212.35	$0.29^{+0.01}_{-0.01}$	$-1.07^{+0.12}_{-0.12}$	$-0.20^{+0.29}_{-0.36}$	$0.70^{+0.05}_{-0.05}$	No
f_{gas}^{ACT} +H(z)+BAO+P1	229.97	$0.30^{+0.01}_{-0.01}$	$-1.06^{+0.11}_{-0.11}$	$0.08^{+0.20}_{-0.22}$	$0.68^{+0.05}_{-0.05}$	No

Table C2. The same as Table C1 for the BA parameterization.

FSLLI parameterization						
Data set	χ_{min}^2	Ω_m	w_0	w_1	z_t	z_{sd}
H(z)+BAO+W9	49.24	$0.28^{+0.01}_{-0.01}$	$-1.27^{+0.20}_{-0.19}$	$0.40^{+0.68}_{-0.78}$	$0.64^{+0.06}_{-0.06}$	No
H(z)+BAO+P1	67.01	$0.29^{+0.01}_{-0.01}$	$-1.22^{+0.18}_{-0.17}$	$0.32^{+0.54}_{-0.57}$	$0.63^{+0.05}_{-0.05}$	No
A04						
$f_{\text{gas}}^{\text{Allen}}$	41.75	$0.28^{+0.03}_{-0.03}$	$-0.79^{+0.48}_{-0.49}$	$-2.77^{+2.90}_{-3.07}$	$0.69^{+0.10}_{-0.10}$	$0.21^{+0.07}_{-0.09}$ (2.6)
$f_{\text{gas}}^{\text{ACT}}$	161.59	$0.31^{+0.02}_{-0.03}$	$-0.74^{+0.30}_{-0.31}$	$-1.83^{+1.32}_{-1.30}$	$0.75^{+0.08}_{-0.08}$	$0.24^{+0.08}_{-0.11}$ (2.5)
$f_{\text{gas}}^{\text{Allen}} + \text{H}(z) + \text{BAO} + \text{W9}$	91.35	$0.28^{+0.01}_{-0.01}$	$-1.27^{+0.18}_{-0.17}$	$0.36^{+0.64}_{-0.73}$	$0.64^{+0.06}_{-0.06}$	No
$f_{\text{gas}}^{\text{Allen}} + \text{H}(z) + \text{BAO} + \text{P1}$	109.22	$0.28^{+0.01}_{-0.01}$	$-1.23^{+0.16}_{-0.15}$	$0.36^{+0.50}_{-0.52}$	$0.63^{+0.05}_{-0.05}$	No
$f_{\text{gas}}^{\text{ACT}} + \text{H}(z) + \text{BAO} + \text{W9}$	212.60	$0.29^{+0.01}_{-0.01}$	$-1.13^{+0.18}_{-0.17}$	$-0.15^{+0.67}_{-0.74}$	$0.68^{+0.04}_{-0.06}$	No
$f_{\text{gas}}^{\text{ACT}} + \text{H}(z) + \text{BAO} + \text{P1}$	231.23	$0.29^{+0.009}_{-0.009}$	$-1.16^{+0.15}_{-0.14}$	$0.07^{+0.49}_{-0.52}$	$0.66^{+0.05}_{-0.05}$	No
A08						
$f_{\text{gas}}^{\text{Allen}}$	41.86	$0.29^{+0.03}_{-0.04}$	$-0.83^{+0.48}_{-0.50}$	$-2.29^{+2.56}_{-2.87}$	$0.69^{+0.14}_{-0.13}$	$0.23^{+0.12}_{-0.10}$ (2.0)
$f_{\text{gas}}^{\text{ACT}}$	174.33	$0.31^{+0.02}_{-0.03}$	$-0.83^{+0.29}_{-0.26}$	$-0.92^{+1.01}_{-1.28}$	$0.73^{+0.10}_{-0.13}$	$0.26^{+0.08}_{-0.11}$ (2.7)
$f_{\text{gas}}^{\text{Allen}} + \text{H}(z) + \text{BAO} + \text{W9}$	91.33	$0.28^{+0.01}_{-0.01}$	$-1.25^{+0.18}_{-0.17}$	$0.31^{+0.66}_{-0.74}$	$0.64^{+0.06}_{-0.06}$	No
$f_{\text{gas}}^{\text{Allen}} + \text{H}(z) + \text{BAO} + \text{P1}$	109.01	$0.28^{+0.01}_{-0.01}$	$-1.22^{+0.16}_{-0.16}$	$0.31^{+0.52}_{-0.54}$	$0.64^{+0.05}_{-0.05}$	No
$f_{\text{gas}}^{\text{ACT}} + \text{H}(z) + \text{BAO} + \text{W9}$	212.35	$0.29^{+0.01}_{-0.01}$	$-1.07^{+0.12}_{-0.12}$	$-0.20^{+0.29}_{-0.36}$	$0.67^{+0.05}_{-0.06}$	No
$f_{\text{gas}}^{\text{ACT}} + \text{H}(z) + \text{BAO} + \text{P1}$	229.97	$0.30^{+0.01}_{-0.01}$	$-1.06^{+0.11}_{-0.11}$	$-0.08^{+0.20}_{-0.22}$	$0.66^{+0.05}_{-0.05}$	No

Table C3. The same as Table C1 for the FSLLI parameterization.

FSLLI parameterization						
Data set	χ_{min}^2	Ω_m	w_0	w_1	z_t	z_{sd}
H(z)+BAO+W9	49.82	$0.29^{+0.01}_{-0.01}$	$-1.13^{+0.10}_{-0.10}$	$-0.36^{+0.58}_{-0.74}$	$0.71^{+0.06}_{-0.05}$	No
H(z)+BAO+P1	67.61	$0.29^{+0.01}_{-0.01}$	$-1.09^{+0.10}_{-0.10}$	$-0.13^{+0.39}_{-0.44}$	$0.69^{+0.05}_{-0.04}$	No
A04						
$f_{\text{gas}}^{\text{Allen}}$	41.50	$0.28^{+0.02}_{-0.02}$	$-1.05^{+0.25}_{-0.27}$	$-4.58^{+4.07}_{-3.64}$	$0.72^{+0.11}_{-0.13}$	No
$f_{\text{gas}}^{\text{ACT}}$	161.64	$0.31^{+0.02}_{-0.03}$	$-0.99^{+0.17}_{-0.18}$	$-2.54^{+1.95}_{-2.41}$	$0.75^{+0.10}_{-0.10}$	No
$f_{\text{gas}}^{\text{Allen}} + \text{H}(z) + \text{BAO} + \text{W9}$	91.95	$0.29^{+0.01}_{-0.01}$	$-1.15^{+0.09}_{-0.09}$	$-0.30^{+0.56}_{-0.72}$	$0.70^{+0.05}_{-0.05}$	No
$f_{\text{gas}}^{\text{Allen}} + \text{H}(z) + \text{BAO} + \text{P1}$	109.98	$0.29^{+0.01}_{-0.01}$	$-1.12^{+0.09}_{-0.09}$	$-0.05^{+0.36}_{-0.40}$	$0.68^{+0.04}_{-0.03}$	No
$f_{\text{gas}}^{\text{ACT}} + \text{H}(z) + \text{BAO} + \text{W9}$	212.28	$0.29^{+0.01}_{-0.01}$	$-1.12^{+0.08}_{-0.07}$	$-0.55^{+0.58}_{-0.76}$	$0.72^{+0.05}_{-0.05}$	No
$f_{\text{gas}}^{\text{ACT}} + \text{H}(z) + \text{BAO} + \text{P1}$	231.34	$0.29^{+0.007}_{-0.007}$	$-1.13^{+0.07}_{-0.07}$	$-0.09^{+0.34}_{-0.39}$	$0.69^{+0.04}_{+0.03}$	No
A08						
$f_{\text{gas}}^{\text{Allen}}$	41.60	$0.29^{+0.03}_{-0.04}$	$-1.04^{+0.29}_{-0.32}$	$-4.30^{+3.87}_{-3.72}$	$0.69^{+0.14}_{-0.16}$	No
$f_{\text{gas}}^{\text{ACT}}$	170.02	$0.31^{+0.02}_{-0.03}$	$-0.95^{+0.16}_{-0.17}$	$-1.94^{+2.25}_{-3.38}$	$0.73^{+0.12}_{-0.17}$	No
$f_{\text{gas}}^{\text{Allen}} + \text{H}(z) + \text{BAO} + \text{W9}$	91.64	$0.29^{+0.01}_{-0.01}$	$-1.14^{+0.10}_{-0.09}$	$-0.36^{+0.57}_{-0.76}$	$0.71^{+0.06}_{-0.05}$	No
$f_{\text{gas}}^{\text{Allen}} + \text{H}(z) + \text{BAO} + \text{P1}$	109.53	$0.29^{+0.01}_{-0.01}$	$-1.11^{+0.09}_{-0.09}$	$-0.08^{+0.36}_{-0.40}$	$0.68^{+0.05}_{-0.03}$	No
$f_{\text{gas}}^{\text{ACT}} + \text{H}(z) + \text{BAO} + \text{W9}$	211.99	$0.29^{+0.01}_{-0.01}$	$-1.08^{+0.08}_{-0.08}$	$-0.57^{+0.55}_{-0.73}$	$0.73^{+0.05}_{-0.05}$	No
$f_{\text{gas}}^{\text{ACT}} + \text{H}(z) + \text{BAO} + \text{P1}$	229.97	$0.30^{+0.01}_{-0.01}$	$-1.06^{+0.08}_{-0.08}$	$-0.25^{+0.35}_{-0.38}$	$0.69^{+0.05}_{-0.04}$	No

Table C4. The same as Table C1 for the FSLLI parameterization.

SL parameterization						
Data set	χ_{min}^2	Ω_m	w_0	w_1	z_t	z_{sd}
H(z)+BAO+W9	50.01	$0.29^{+0.01}_{-0.01}$	$-1.13^{+0.15}_{-0.14}$	$-1.20^{+0.09}_{-0.12}$	$0.69^{+0.05}_{-0.04}$	No
H(z)+BAO+P1	68.52	$0.29^{+0.01}_{-0.01}$	$-1.10^{+0.13}_{-0.13}$	$-1.13^{+0.05}_{-0.05}$	$0.68^{+0.04}_{-0.03}$	No
A04						
f_{gas}^{Allen}	41.71	$0.28^{+0.03}_{-0.03}$	$-0.83^{+0.50}_{-0.56}$	$-1.92^{+0.93}_{-1.02}$	$0.67^{+0.12}_{-0.15}$	$0.24^{+0.12}_{-0.11}$ (2.0)
f_{gas}^{ACT}	161.64	$0.31^{+0.02}_{-0.03}$	$-0.81^{+0.27}_{-0.27}$	$-1.48^{+0.28}_{-0.29}$	$0.76^{+0.09}_{-0.09}$	$0.25^{+0.09}_{-0.13}$ (2.2)
$f_{gas}^{Allen}+H(z)+BAO+W9$	92.11	$0.28^{+0.01}_{-0.01}$	$-1.15^{+0.12}_{-0.12}$	$-1.21^{+0.09}_{-0.12}$	$0.69^{+0.05}_{-0.04}$	No
$f_{gas}^{Allen}+H(z)+BAO+P1$	110.97	$0.29^{+0.01}_{-0.01}$	$-1.13^{+0.12}_{-0.12}$	$-1.13^{+0.04}_{-0.50}$	$0.67^{+0.04}_{-0.03}$	No
$f_{gas}^{ACT}+H(z)+BAO+W9$	212.46	$0.29^{+0.01}_{-0.01}$	$-1.08^{+0.13}_{-0.11}$	$-1.23^{+0.09}_{-0.11}$	$0.71^{+0.04}_{-0.04}$	No
$f_{gas}^{ACT}+H(z)+BAO+P1$	231.91	$0.29^{+0.008}_{-0.008}$	$-1.12^{+0.10}_{-0.10}$	$-1.15^{+0.04}_{-0.05}$	$0.68^{+0.04}_{-0.03}$	No
A08						
f_{gas}^{Allen}	41.76	$0.29^{+0.03}_{-0.04}$	$-0.87^{+0.50}_{-0.54}$	$-1.76^{+0.77}_{-0.93}$	$0.66^{+0.15}_{-0.18}$	$0.25^{+0.13}_{-0.12}$ (2.0)
f_{gas}^{ACT}	179.20	$0.31^{+0.02}_{-0.04}$	$-0.79^{+0.32}_{-0.29}$	$-1.39^{+0.42}_{-0.49}$	$0.74^{+0.11}_{-0.15}$	$0.27^{+0.09}_{-0.13}$ (2.4)
$f_{gas}^{Allen}+H(z)+BAO+W9$	91.87	$0.29^{+0.01}_{-0.01}$	$-1.13^{+0.13}_{-0.13}$	$-1.21^{+0.09}_{-0.12}$	$0.69^{+0.05}_{-0.04}$	No
$f_{gas}^{Allen}+H(z)+BAO+P1$	110.27	$0.29^{+0.01}_{-0.01}$	$-1.11^{+0.12}_{-0.12}$	$-1.13^{+0.05}_{-0.05}$	$0.67^{+0.04}_{-0.03}$	No
$f_{gas}^{ACT}+H(z)+BAO+W9$	212.29	$0.29^{+0.01}_{-0.01}$	$-1.05^{+0.13}_{-0.12}$	$-1.20^{+0.10}_{-0.12}$	$0.71^{+0.05}_{-0.05}$	No
$f_{gas}^{ACT}+H(z)+BAO+P1$	230.83	$0.30^{+0.01}_{-0.01}$	$-1.04^{+0.11}_{-0.11}$	$-1.12^{+0.05}_{-0.05}$	$0.69^{+0.04}_{-0.04}$	No

Table C5. The same as Table C1 for the SL parameterization.

z	$H(z)$	σ_H	Reference	Method
0.07	69	19.6	Zhang et al. (2012)	DA
0.1	69	12	Stern et al. (2010)	DA
0.12	68.6	26.2	Zhang et al. (2012)	DA
0.17	83	8	Stern et al. (2010)	DA
0.179	75	4	Moresco et al. (2012)	DA
0.199	75	5	Moresco et al. (2012)	DA
0.2	72.9	29.6	Zhang et al. (2012)	DA
0.24	79.69	2.65	Gaztanaga et al. (2009)	Clustering
0.27	77	14	Stern et al. (2010)	DA
0.28	88.8	36.6	Zhang et al. (2012)	DA
0.3	81.7	6.22	Oka et al. (2014)	Clustering
0.35	82.7	8.4	Chuang & Wang (2013)	Clustering
0.352	83	14	Moresco et al. (2012)	DA
0.4	95	17	Stern et al. (2010)	DA
0.43	86.45	3.68	Gaztanaga et al. (2009)	Clustering
0.44	82.6	7.8	Blake et al. (2012)	Clustering
0.48	97	62	Stern et al. (2010)	DA
0.57	92.9	7.8	Anderson et al. (2014)	Clustering
0.593	104	13	Moresco et al. (2012)	DA
0.600	87.9	6.1	Blake et al. (2012)	Clustering
0.68	92	8	Moresco et al. (2012)	DA
0.73	97.3	7	Blake et al. (2012)	Clustering
0.781	105	12	Moresco et al. (2012)	DA
0.875	125	17	Moresco et al. (2012)	DA
0.88	90	40	Stern et al. (2010)	DA
0.9	117	23	Stern et al. (2010)	DA
1.037	154	20	Moresco et al. (2012)	DA
1.3	168	17	Stern et al. (2010)	DA
1.43	177	18	Stern et al. (2010)	DA
1.53	140	14	Stern et al. (2010)	DA
1.75	202	40	Stern et al. (2010)	DA
2.3	224	8	Busca et al. (2013)	Clustering
2.34	222	7	Delubac et al. (2014)	Clustering
2.36	226	8	Font-Ribera et al. (2014)	Clustering

Table D1. Hubble parameter measurements $H(z)$ (in $\text{km s}^{-1}\text{Mpc}^{-1}$) and its error, σ_H , at redshift z . The method refers to as $H(z)$ was obtained: DA stands for diameter angular distance.

JBP parameterization

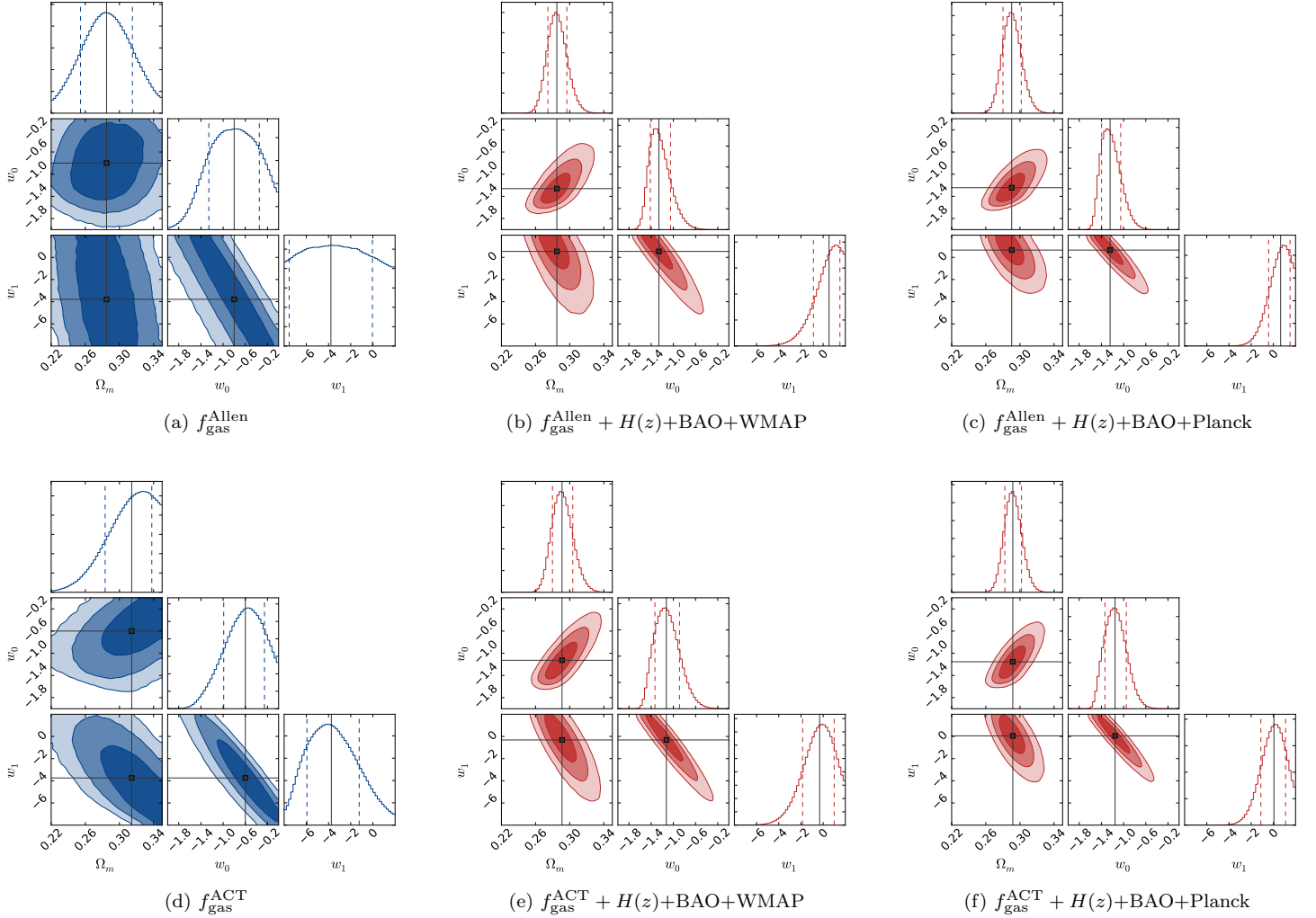
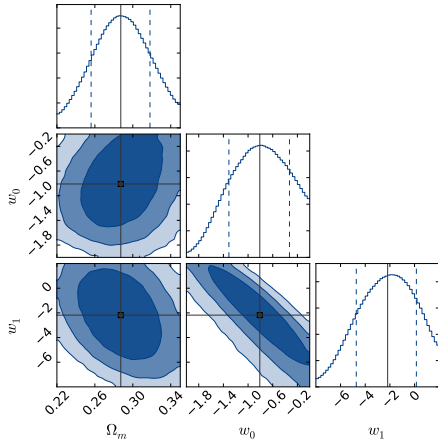
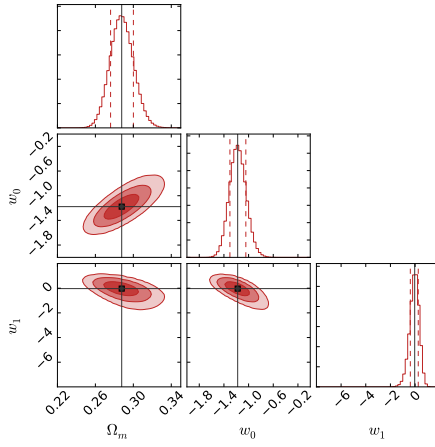


Figure C1. 1D marginalized posterior distributions and 2D 68%, 95%, 99% confidence levels for the Ω_m , w_0 , and w_1 parameters of the JBP parameterization. The top-left panel shows the confidence regions obtained using the $f_{\text{gas}}^{\text{Allen}}$ data alone. The top-middle and top-right panels show the same contours computed from the $f_{\text{gas}}^{\text{Allen}} + H(z)+\text{BAO}+\text{CMB}$ joint analysis using WMAP and Planck data respectively. The bottom panels show the same as the top panels obtained using the $f_{\text{gas}}^{\text{ACT}}$ data. The squares show the best fit values.

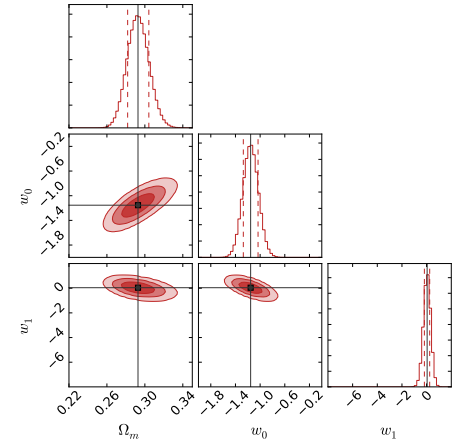
BA parameterization



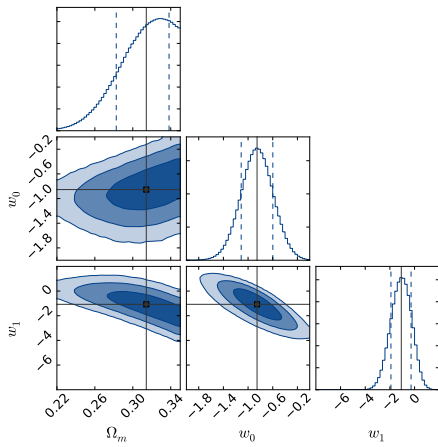
(a) $f_{\text{gas}}^{\text{Allen}}$



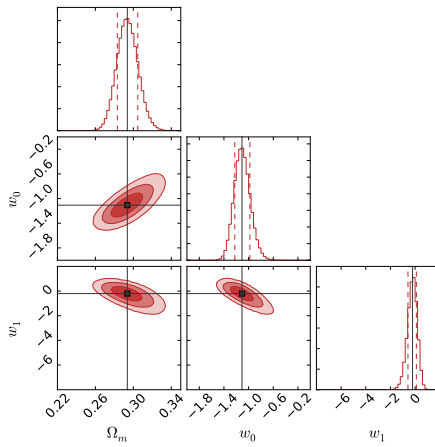
(b) $f_{\text{gas}}^{\text{Allen}} + H(z)+\text{BAO}+\text{WMAP}$



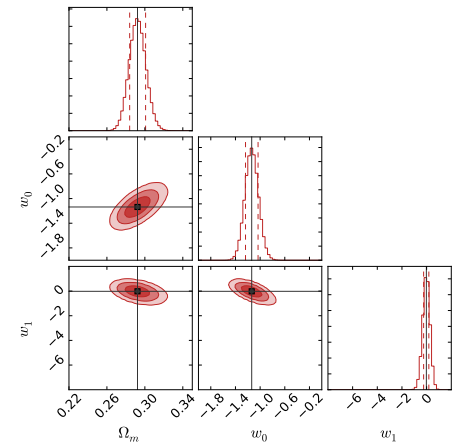
(c) $f_{\text{gas}}^{\text{Allen}} + H(z)+\text{BAO}+\text{Planck}$



(d) $f_{\text{gas}}^{\text{ACT}}$



(e) $f_{\text{gas}}^{\text{ACT}} + H(z)+\text{BAO}+\text{WMAP}$



(f) $f_{\text{gas}}^{\text{ACT}} + H(z)+\text{BAO}+\text{Planck}$

Figure C2. The same as Fig. C1 for the BA parameterization.

FSLLI parameterization

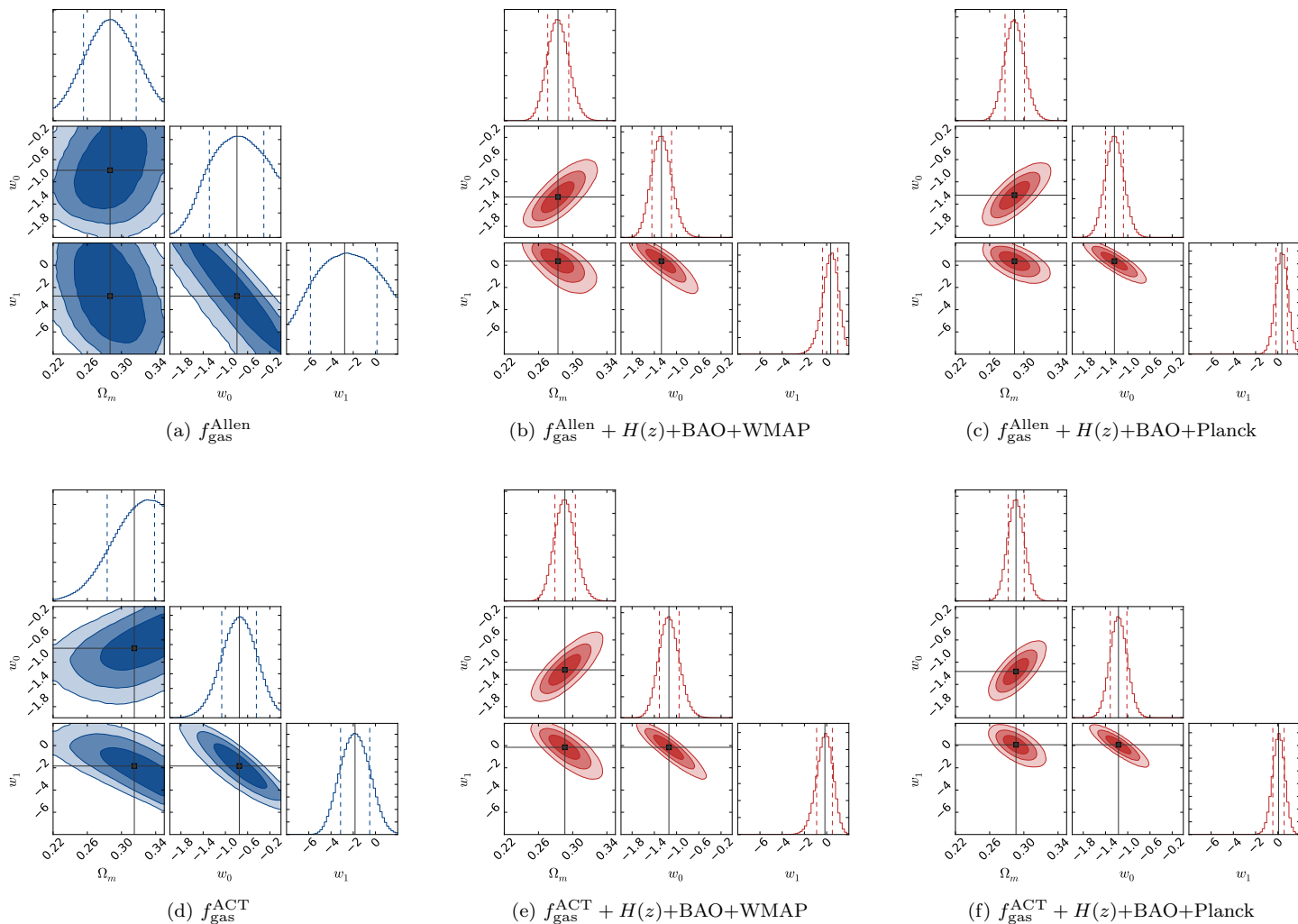


Figure C3. The same as Fig. C1 for the FSLLI parameterization.

FSLII parameterization

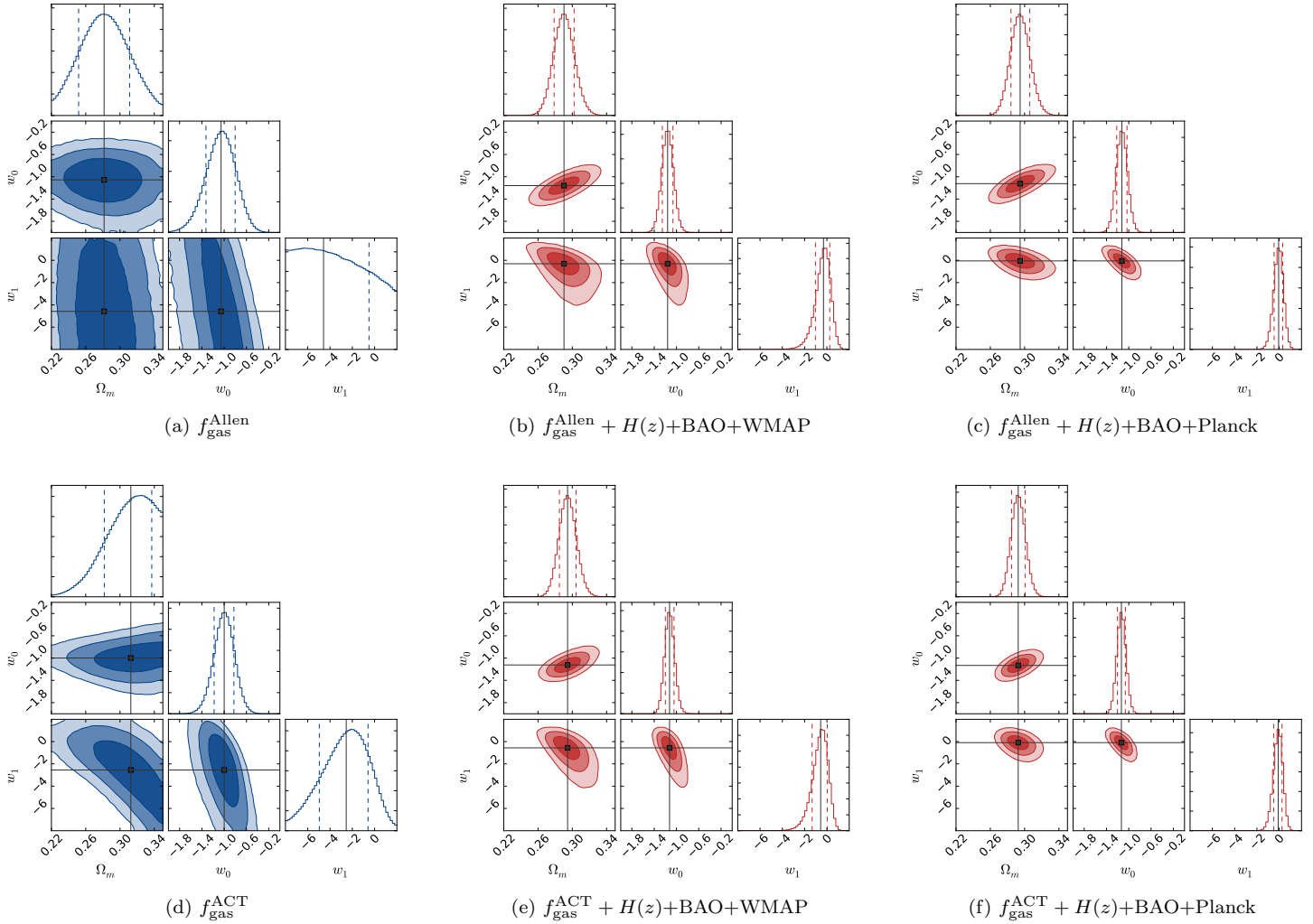


Figure C4. The same as Fig. C1 for the FSLII parameterization.

SL parameterization

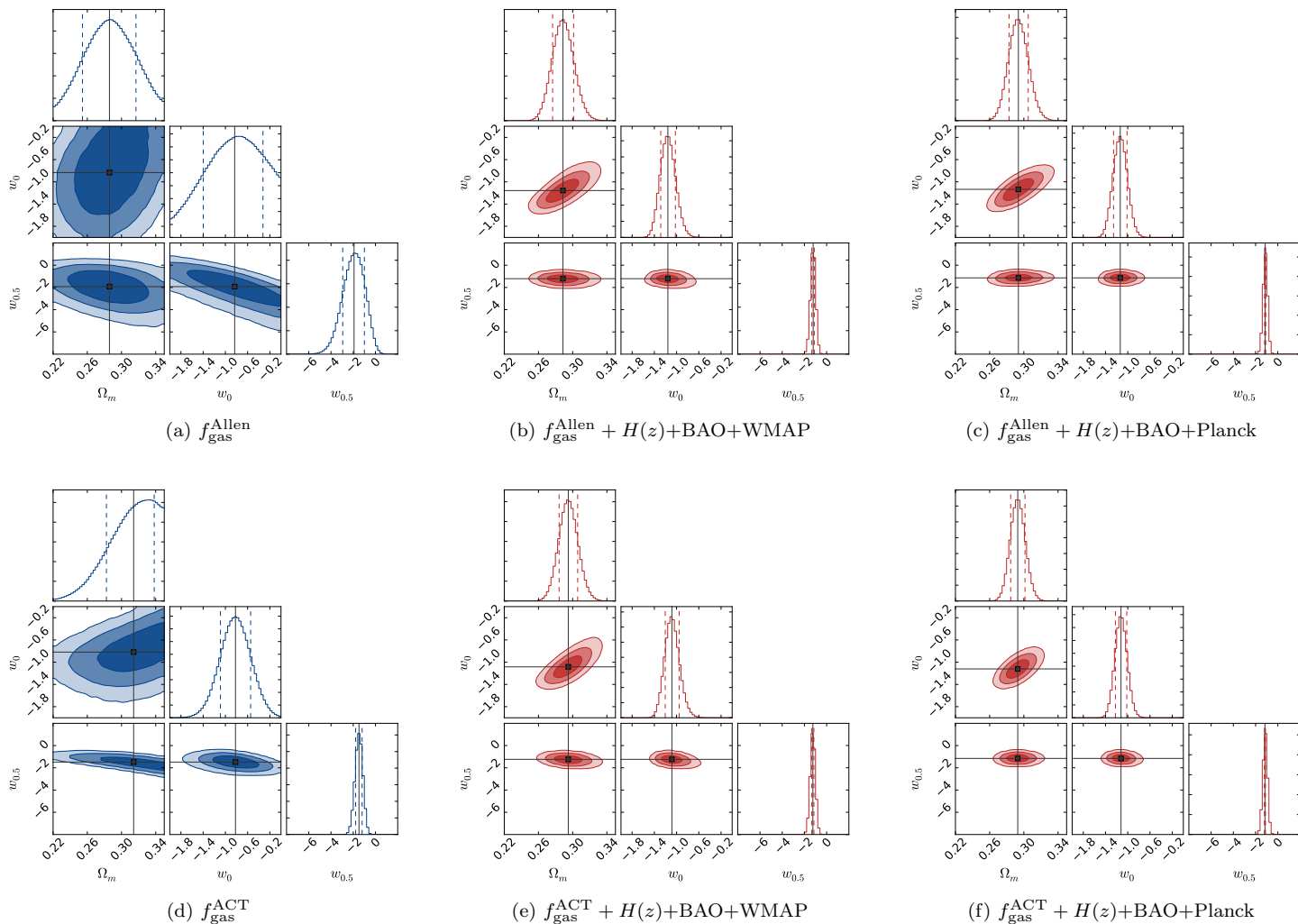


Figure C5. The same as Fig. C1 for the SL parameterization.